Discrete Connection and Covariant Derivative for Vector Field Analysis and Design

BEIBEI LIU and YIYING TONG
Michigan State University
and
FERNANDO DE GOES and MATHIEU DESBRUN
California Institute of Technology

In this article, we introduce a discrete definition of connection on simplicial manifolds, involving closed-form continuous expressions within simplices and finite rotations across simplices. The finite-dimensional parameters of this connection are optimally computed by minimizing a quadratic measure of the deviation to the (discontinuous) Levi-Civita connection induced by the embedding of the input triangle mesh, or to any metric connection with arbitrary cone singularities at vertices. From this discrete connection, a covariant derivative is constructed through exact differentiation, leading to explicit expressions for local integrals of first-order derivatives (such as divergence, curl, and the Cauchy-Riemann operator) and for L_2-based energies (such as the Dirichlet energy). We finally demonstrate the utility, flexibility, and accuracy of our discrete formulations for the design and analysis of vector, n-vector, and n-direction fields.

CCS Concepts: • **Computing methodologies → Mesh models**

Additional Key Words and Phrases: Vector field design, covariant derivative, discrete connection, discrete differential geometry

ACM Reference Format:

Beibei Liu, Yiying Tong, Fernando de Goes, and Mathieu Desbrun. 2016. Discrete connection and covariant derivative for vector field analysis and design. ACM Trans. Graph. 35, 3, Article 23 (March 2016), 17 pages.
DOI: http://dx.doi.org/10.1145/2870629

1. INTRODUCTION

Established by Ricci and Levi-Civita, covariant differentiation is a central concept in differential geometry that measures the rate of change of a (tangent) vector field over a curved surface. The covariant derivative can thus quantify the smoothness of a vector field, evaluate its local fluxes, and even identify its singularities. Consequently, discretizing the notion of covariant derivative is crucial to digital geometry processing, with applications ranging from texture synthesis to shape analysis, meshing, and simulation. However, existing discrete counterparts of such a differential operator acting on simplicial manifolds can either approximate local derivatives (such as divergence and curl) or estimate global integrals (such as the Dirichlet energy), but not both simultaneously.

In this article, we present a unified discretization of the covariant derivative that offers closed-form expressions for both local and global first-order derivatives of vertex-based tangent vector fields on triangulations. Our approach is based on a new construction of discrete connections that provides consistent interpolation of tangent vectors within and across mesh simplices while minimizing the deviation to the Levi-Civita connection induced by the 3D embedding of the input mesh—or, more generally, to any metric connection with arbitrary cone singularities at vertices. We demonstrate the relevance of our contributions by providing new computational tools to design and edit vector and n-direction fields.

1.1 Previous Work

While many graphics applications (from texture synthesis to fluid animation) make use of discrete vector fields, we only review previous methods that have addressed the analysis and design of vector and n-direction fields over triangulated surfaces.

Vector fields. Computational tools for vector fields on triangle meshes are required whether the user is given a tangent vector field to analyze or whether he or she needs to design a vector field from a sparse set of desired constraints. For instance, discrete notions of divergence and curl (vorticity) were formulated [Polthier and Preuß 2003; Tong et al. 2003]; topological analysis also attracted interest, resulting in methods in which positions of vector field singularities are identified, merged, split, or moved [Theisel 2002; Zhang et al. 2006]. Quadratic energies measuring vector field smoothness were also introduced since their minimizers (possibly with added user constraints) limit the appearance of singularities [Fisher et al. 2007].

From vector fields to n-direction fields. The more general case of n-direction fields (called unit n rotational symmetry (RoSy) fields in Palacios and Zhang [2007]) such as direction fields ($n = 2$) or cross-fields ($n = 4$) were numerically handled through energy minimization as well, but the energies that were initially proposed for this case were highly nonlinear [Hertzmann and Zorin 2000; Palacios and Zhang 2007; Ray et al. 2008] or involved integer variables [Ray et al. 2009; Bommes et al. 2009; Panozzo et al. 2012]. A quadratic energy was recently introduced in Knöppel et al. [2013] through a discretized version of the Dirichlet energy, extending the

Authors' addresses: B. Liu and M. Desbrun, Caltech MS 305-16, Pasadena, CA 91125; emails: {liubeibe, mathieu}@caltech.edu; Y. Tong, MSU Engineering Building, 428 S. Shaw Lane #3115, East Lansing, MI 48824; email: ytong@msu.edu; F. de Goes, Pixar Animation Studios, 1200 Park Avenue, Emeryville, California 94608; email: fernando@pixar.com.

DOI: http://dx.doi.org/10.1145/2870629

method of Fisher et al. [2007], which only accounted for the squared sum of the divergence and of the curl of vector fields over the surface. The extra curvature and boundary terms of this new approach were also shown to offer additional user control. Nonintersecting integral lines of such n-RoSy fields can then be constructed through Ray and Sokolov [2014] and Myles et al. [2014] for applications such as global parameterization.

Connections. The importance of connections in geometry processing was noted early on, even in applications unrelated to field design. Intuitively, a connection prescribes (in a given local frame field) how the frame at one point should be modified to produce a "parallel" frame at a nearby point, so as to allow the comparison between vectors in nearby frames. For instance, Lipman et al. [2005] used what conceptually amounted to Christoffel symbols between vertex-based tangent planes to describe the effects of parallel transport in an effort to introduce linear rotation-invariant coordinates; however, these coefficients end up bearing little resemblance to their continuous equivalents. Kircher and Garland [2008] proposed to use a triangle-to-triangle connection in the context of free-form deformation, but no notion of differentiation was discussed. A formal discrete version of connections between triangles was defined in Crane et al. [2010], encoding the alignment angle for parallel transport from one triangle to an adjacent one, and with which piecewise-constant unit vector and n-direction fields can be derived for any given set of singularities. The recent work of Knöppel et al. [2013], instead, used a notion of parallel transport through the blending of geodesic polar maps similar to Zhang et al. [2006], which determines a connection between vertices as opposed to triangles. This approach results in a continuous notion of vector fields (and n-vector fields) compared to the piecewise constant discretization per face of Crane et al. [2010], Wang et al. [2012], and Myles and Zorin [2013], and thus allows a formal evaluation of the Dirichlet energy. Their choice of connection is based on the even distribution of the Gaussian curvature of the input mesh from vertices to faces, which leads to closed-form expressions of the L_2 integrals they sought. However, the deviation (and thus the discretization error) of their connection from the canonical Levi-Civita connection of the mesh embedded in $\mathbb{R}^3$ is difficult to quantify since no closed-form expression of the covariant derivative itself was provided. Additionally, first-order derivative operators such as divergence or curl *cannot* be evaluated in their framework—neither pointwise nor as local integrals. The more recent work of de Goes et al. [2014] provided discrete covariant derivatives induced by discrete symmetric 2-tensors as a global mapping from a pair of discrete 1-forms to another discrete 1-form but offers no pointwise expressions either.

In conclusion, and despite the fact that vector, n-vector, and n-direction fields over triangulated surfaces have received much attention lately, there is still no existing approach offering discrete operators capturing both local and global differential information in a consistent manner. Moreover, the few existing approaches to connections do not offer a discretization that can be argued to be optimally close to the canonical connection induced by a metric.

1.2 Contributions

In this article, we introduce a notion of discrete connection over simplicial manifolds that offers closed-form expressions for first-order derivatives and L_2-based energies of (n-)vector and n-direction fields. Using one reference frame per simplex, a discrete connection is encoded through *finite rotations* between incident simplices, and through continuous *Whitney connection* 1*-forms* within edges and triangles. A closed-form expression of the covariant derivative is then derived from the connection through direct differentiation, offering pointwise or integral evaluations of first-order operators (such as divergence, curl, and the Cauchy-Riemann operator) and relevant energies (such as the Dirichlet energy). We also propose the computation of an as-Levi-Civita-as-possible discrete connection through a linear solve, defining a finite-dimensional connection that deviates the least (in a norm defined later) from the original connection induced by the embedding of the mesh in $\mathbb{R}^3$. Significant numerical improvements over previous methods are obtained for analytical vector fields when this as-Levi-Civita-as-possible discrete connection is used for discrete operators on vector fields. Our representation is extended to handle any metric connection with arbitrary cone singularities at vertices as well. We also demonstrate the relevance and practical use of our discrete connections by contributing *new numerical tools* for n-vector field editing that control the position *and* orientation of both positive *and* negative singularities.

1.3 Outline and Notations

We first review the continuous definitions and relevant properties of connections, covariant derivatives, and associated energies in Section 2. We describe the rationale behind our construction of vertex-based vector fields on meshes via a discrete connection in Section 3. We then elaborate on the discrete definition of connection in Section 4, before discussing in Section 5 how to compute a globally optimal discrete connection in the sense that it is the closest to the Levi-Civita connection of the surface. We further provide in Section 6 closed-form expressions for basis functions of vector fields and covariant derivatives based on our discrete connections, before explaining in Section 7 how these numerical tools can be leveraged to improve (n-)vector and n-direction field editing on triangle meshes. We conclude with visual results of vector field editing and numerical comparisons of our operators in Section 8.

Throughout our exposition, we denote by $\mathcal{T}$ a triangulation of a 2-manifold M of arbitrary topology, with vertices $V = \{v_i\}_i$, edges $E = \{e_{ij}\}_{i,j}$, and triangles $T = \{t_{ijk}\}_{i,j,k}$. Each vertex v_i is assigned a position $\mathbf{p}_i$ in $\mathbb{R}^3$. Each edge further carries an arbitrary but fixed orientation, while vertices and triangles always have counterclockwise orientation by convention. Index order indicates direction, in the sense that edge e_{ij} is directed from vertex v_i to v_j. The bold symbol $\mathbf{e}_{ij}$ will denote the vector formed by edge e_{ij} in its Euclidean embedding space $\mathbb{R}^3$. We exploit the containment relation of a simplicial complex by defining σ to be a *face* of η, and η a *coface* of σ, if and only if $\sigma \subset \eta$ with $\sigma, \eta \in \mathcal{T}$. We denote the angle in a triangle t_{ijk} between jk and ji by $\theta_{ijk} > 0$. The discrete Gaussian curvature of $\mathcal{T}$ at a vertex v_i is thus expressed as $\kappa_i = 2\pi - \sum_{t_{ijk}} \theta_{kij}$. Finally, we denote by φ_i, φ_{ij}, and φ_{ijk} the Whitney bases of 0-forms on vertices v_i, 1-forms on edges e_{ij}, and 2-forms on triangles t_{ijk}, respectively [Whitney 1957; Desbrun et al. 2008]. The piecewise-linear basis function φ_i is supported over the one-ring of v_i, satisfying $\varphi_i(v_j) = \delta_{ij}$ (where δ is the Kronecker symbol) and offering a partition of unity ($\varphi_i + \varphi_j + \varphi_k = 1$) on triangle ijk. The other bases are defined as $\varphi_{ij} = \varphi_i d\varphi_j - \varphi_j d\varphi_i$, and $\varphi_{ijk} = 2\, d\varphi_i \wedge d\varphi_j$ (where d is akin to gradient and $\wedge$ is akin to cross-product).

2. CONNECTIONS ON SMOOTH MANIFOLDS

We begin our exposition by reviewing continuous geometric notions that will be relevant to our contributions. While these notions can be introduced in various ways, we focus as much as possible on intrinsic definitions as they will be easier to discretize later on.

2.1 Tangent Vector Fields

Consider a compact topological 2-manifold M, covered by a collection (atlas) of charts that have C^∞ smooth transition functions between each overlapping pair (which always exists [Grimm and Hughes 1995; Marathe 2010]). The notion of tangent planes and vectors can be defined intrinsically (i.e., independent of the embedding) via, for instance, the tangency among smooth curves passing through a common point.

Definition 1 *[Abraham et al. 1988].* Let $\mathbf{x} = (x^1, x^2)$ be a local chart mapping an open set $U \subset M$ to $\mathbb{R}^2$. A smooth *curve* c passing through a point $\mathbf{p} \in U$ is a map $c : I \to U$ for which the interval $I \subset \mathbb{R}$ contains 0, $c(0) = \mathbf{p}$, and $\mathbf{x} \circ c$ is C^2. Two smooth curves c_1 and c_2 are said to be **tangent** at $\mathbf{p}$ if and only if

$$(\mathbf{x} \circ c_1)'(0) = (\mathbf{x} \circ c_2)'(0). \tag{1}$$

Note that this definition of tangency is independent of the choice of charts. Tangent curves can thus be used as an equivalence relation defining intrinsic vector spaces tangent to M.

Definition 2 *[Abraham et al. 1988].* A **tangent vector** at $\mathbf{p} \in M$ is the equivalence class $[c]_\mathbf{p}$ of curves tangent to curve c at $\mathbf{p}$. The space of tangent vectors is called the **tangent space** at $\mathbf{p}$, denoted as $T_\mathbf{p}M$. The **tangent bundle** is the (disjoint) union of tangent spaces $TM = \cup_{\mathbf{p}\in M} T_\mathbf{p}M$.

When the surface M has an embedding in $\mathbb{R}^3$, one can further express the tangent vectors as 3D vectors orthogonal to the surface normal, as classically explained in differential geometry of surfaces. Observe that the tangent space $T_\mathbf{p}M$ at any point $\mathbf{p} \in M$ is two-dimensional and a tangent vector $\mathbf{u} = [c]_\mathbf{p}$ can be represented in components as $(u^1, u^2) = ((x^1 \circ c)'(0), (x^2 \circ c)'(0))$ in a chart $\mathbf{x}$. Thus, the tangent bundle TM admits the structure of a 4-manifold with charts (x^1, x^2, u^1, u^2) induced by the atlas of M.

Definition 3 *[Abraham et al. 1988].* A (tangent) **vector field** $\mathbf{u}$ is a continuous map $M \to TM$ from a point $\mathbf{p} \in M$ to a vector $\mathbf{u}(\mathbf{p}) \in T_\mathbf{p}M$. A **local frame field** of M on a chart is defined as two vector fields $(\mathbf{e}_1, \mathbf{e}_2)$ that are linearly independent pointwise.

Global frame fields do not exist in general; otherwise, one could build a continuous vector field that is nonzero everywhere on a genus-0 surface, thus contradicting the hairy ball theorem [Spivak 1979]. Consequently, TM does not usually have the structure of $M \times \mathbb{R}^2$. On a chart with a local frame field, a vector field $\mathbf{u}$ can be expressed in components as

$$\mathbf{u} = u^1\mathbf{e}_1 + u^2\mathbf{e}_2. \tag{2}$$

The aforementioned chart of TM can be seen as a special case of the component representation, with $\mathbf{e}_i$ (often denoted as $\partial/\partial x^i$) being the equivalence class of the curves generated by varying coordinate x^i while keeping the other coordinate fixed.

Definition 4 *[Abraham et al. 1988].* A **covector** ω at $\mathbf{p}$ is defined as a linear map $\omega : T_\mathbf{p}M \to \mathbb{R}$. The space of covectors is denoted as $T^*_\mathbf{p}M$.

One can likewise define smooth fields of covectors, which are also called (differential) 1-forms. They can be represented in local bases (η^1, η^2) defined by $\eta^i(\mathbf{e}_j) = \delta^i_j$ given a frame field $(\mathbf{e}_1, \mathbf{e}_2)$.

One can also augment a surface M with a metric by assigning an inner product (symmetric positive definite bilinear mapping) $\langle \cdot, \cdot \rangle_\mathbf{p}$ for every tangent space $T_\mathbf{p}M$—for example, for an embedded surface, it can be defined by the inner product of the corresponding 3D vectors in the 3D Euclidean space.

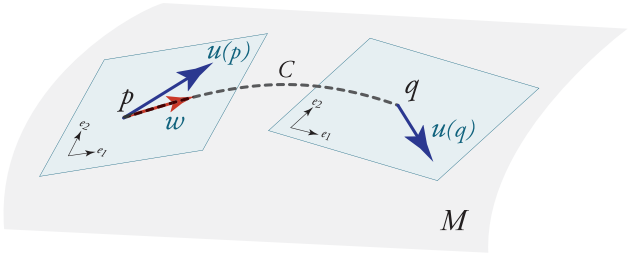

Fig. 1. **Smooth connection.** On a smooth manifold, a connection indicates how a tangent vector at point $\mathbf{p}$ is parallel transported along a path C to a nearby point $\mathbf{q}$, accounting for the change of frame between the two tangent spaces. From a connection the notion of (covariant) derivative of vector fields is deduced, as nearby vectors can now be compared.

Finally, we point out that the directional derivative of a function f over M w.r.t. a vector $\mathbf{u} = [c]_\mathbf{p} \in T_\mathbf{p}M$ is defined as $(f \circ c)'(0)$, corresponding to $df(\mathbf{u})$ in the language of differential forms and to the more familiar inner product $\langle \nabla f, \mathbf{u} \rangle$ when a metric is available [Abraham et al. 1988].

2.2 Covariant Derivative

In order to take derivatives of vector fields, one must account for the fact that vectors in nearby tangent spaces are expressed in different local frames. The concept of covariant differentiation, denoted ∇, provides a principled way to compare nearby tangent vectors and measure their differences. The basic geometric intuition behind the covariant derivative of a vector field $\mathbf{u}$ at a point $\mathbf{p}$ is that $\nabla\mathbf{u}$ encodes the rate of change of $\mathbf{u}$ around $\mathbf{p}$. Projecting the derivative of a vector field $\mathbf{u}$ along a vector $\mathbf{w}$ leads to a vector $\nabla_\mathbf{w}\mathbf{u}$, which indicates the difference between vectors $\mathbf{u}(\mathbf{p})$ at $\mathbf{p}$ and $\mathbf{u}(\mathbf{q})$ at a nearby point $\mathbf{q} \equiv c(\epsilon)$, where c is a curve passing through $\mathbf{p}$ in the equivalence class $\mathbf{w}$, and $\epsilon \in \mathbb{R}$ is small (Figure 1). However, these vectors live in different tangent spaces, so the component-wise differences depend on the choice of local basis frames, and taking their differences in a manner that is purely intrinsic (i.e., coordinate/frame independent) requires the additional notion of connection.

Definition 5 *[Spivak 1979].* A **covariant derivative** (or an **affine connection**) is an operator ∇ mapping a vector $\mathbf{w} \in T_\mathbf{p}M$ and a vector field $\mathbf{u}$ to a vector $\nabla_\mathbf{w}\mathbf{u} \in T_\mathbf{p}M$, so that it is linear in both $\mathbf{u}$ and $\mathbf{w}$ and satisfies Leibniz's product rule; that is, for a vector field $\mathbf{u}$ and a smooth function f, one has

$$\nabla_\mathbf{w}(f\mathbf{u}) = df(\mathbf{w})\mathbf{u} + f\nabla_\mathbf{w}\mathbf{u}.$$

Using the representation of the vector field $\mathbf{u}$ in a local frame field $(\mathbf{e}_1, \mathbf{e}_2)$, we can expand the covariant derivative through linearity and product rule in $\mathbf{u}$ as

$$\nabla_\mathbf{w}\mathbf{u} = \sum_{i=1,2} \left[du^i(\mathbf{w})\mathbf{e}_i + u^i \nabla_\mathbf{w}\mathbf{e}_i \right],$$

where the second term of this derivative accounts for the alignment of the local frame at a point to a nearby local frame along a curve having $\mathbf{w}$ as its tangent vector (Figure 1). By linearity in $\mathbf{w}$, we can rewrite $\nabla_\mathbf{w}\mathbf{e}_i = w^1\nabla_{\mathbf{e}_1}\mathbf{e}_i + w^2\nabla_{\mathbf{e}_2}\mathbf{e}_i$. Now we introduce coefficients ω^k_{ji} satisfying

$$\nabla_{\mathbf{e}_j}\mathbf{e}_i = \omega^1_{ji}\mathbf{e}_1 + \omega^2_{ji}\mathbf{e}_2.$$

In the dual basis (η^1, η^2) of $T^*_\mathbf{p}M$, we can group these coefficients as *local* 1-forms $\omega^i_j \equiv \omega^i_{1j}\eta^1 + \omega^i_{2j}\eta^2$ to encode the alignment of

nearby local frames as a local *matrix-valued* 1-*form*:

$$\Omega(\mathbf{w}) = \begin{pmatrix} \omega_1^1(\mathbf{w}) & \omega_2^1(\mathbf{w}) \\ \omega_1^2(\mathbf{w}) & \omega_2^2(\mathbf{w}) \end{pmatrix}, \ \forall \mathbf{w} \in T_{\mathbf{p}}M.$$

Using Ω, we can reformulate the covariant derivative as

$$\nabla_{\mathbf{w}}\mathbf{u} = (\mathbf{e}_1\ \mathbf{e}_2)\begin{pmatrix} du^1(\mathbf{w}) \\ du^2(\mathbf{w}) \end{pmatrix} + (\mathbf{e}_1\ \mathbf{e}_2)\,\Omega(\mathbf{w})\begin{pmatrix} u^1 \\ u^2 \end{pmatrix}.$$

Note that if one considers a different local frame field $(\tilde{\mathbf{e}}_1, \tilde{\mathbf{e}}_2)$ at $\mathbf{q}$ satisfying $(\tilde{\mathbf{e}}_1(\mathbf{q}), \tilde{\mathbf{e}}_2(\mathbf{q})) = (\mathbf{e}_1(\mathbf{q}), \mathbf{e}_2(\mathbf{q}))(I + \epsilon\Omega(\mathbf{w}))$, where $\mathbf{q} = \mathbf{x}^{-1}(\mathbf{x}(\mathbf{p}) + \epsilon\mathbf{w})$ is a point ϵ-away from $\mathbf{p}$ along $\mathbf{w}$ (still expressed in chart $\mathbf{x}$), then the corresponding matrix-valued 1-form satisfies $\tilde{\Omega}(\mathbf{w}) = 0$, and $\epsilon\nabla_{\mathbf{w}}\mathbf{u}$ becomes a direct comparison of components $(\tilde{u}^1, \tilde{u}^2)$ at $\mathbf{q}$ and $\mathbf{p}$; in other words, these frames are aligned. It is also worth pointing out that, even though the matrix-based 1-form Ω is dependent on the choice of frame field, $\nabla\mathbf{u}$ is instead a proper, globally defined tensor field.

2.3 Metric Connections

While the previous definitions are valid for arbitrary connections, we will restrict our attention from now on to metric affine connections.

Definition 6 *[Spivak 1979].* For a smooth 2-manifold M equipped with a metric $\langle\cdot,\cdot\rangle$, a **metric affine connection** is a connection that preserves the metric, that is, that satisfies

$$d\,\langle \mathbf{u}_1, \mathbf{u}_2\rangle\,(\mathbf{w}) = \langle \nabla_{\mathbf{w}}\mathbf{u}_1, \mathbf{u}_2\rangle + \langle \mathbf{u}_1, \nabla_{\mathbf{w}}\mathbf{u}_2\rangle\ ,\ \forall \mathbf{w}, \mathbf{u}_1, \mathbf{u}_2 \in TM.$$

Note that an orthonormal frame field $(\mathbf{e}_1, \mathbf{e}_2) \equiv (\mathbf{e}, \mathbf{e}^{\perp})$ is uniquely defined through a unit vector $\mathbf{e}$ and its $\pi/2$-rotation $\mathbf{e}^{\perp}$ in the given metric; we thus (by abuse of notation) refer to $\mathbf{e}$ as a local frame field. With the compatibility condition that metric connections must verify, the local 1-form Ω on an orthonormal frame simplifies to

$$\Omega = \begin{pmatrix} 0 & -\omega \\ \omega & 0 \end{pmatrix} = \omega J,$$

where J is the $\pi/2$-rotation matrix

$$J = \begin{pmatrix} 0 & -1 \\ 1 & 0 \end{pmatrix},$$

and ω is a local, real-valued 1-form encoding infinitesimal angular velocity with which a local frame needs to rotate to align to nearby frames when moving along a given vector. We will refer to ω as the (metric) connection 1-form.

An important special case of metric connection is the Levi-Civita connection: for a given metric defined over a 2-manifold M, this is the *unique* metric connection simultaneously preserving this metric *and* satisfying $\omega^i_{jk} = \omega^i_{kj}$ in frame field $(\partial/\partial x^1, \partial/\partial x^2)$. In particular, for a surface embedded in $\mathbb{R}^3$, the Levi-Civita connection induced by the metric inherited from the Euclidean space corresponds to the tangential component of the traditional (3D) component-wise derivatives of a vector field.

As metric connections will be at the core of our contributions, we delve further into related continuous concepts that will be useful in later sections. For definitions of other connections defined on vector or frame bundles, we refer the reader to Spivak [1979].

2.4 Related Concepts

We end this section with a few key geometric definitions that we will refer to extensively in our work.

Parallel transport. The notion of connection allows a natural definition of parallel transport: given a connection 1-form ω and its covariant derivative ∇, the parallel transport of a vector $\mathbf{u}(\mathbf{p})$ along a curve c is defined as vectors along the curve such that $\nabla_{c'(s)}\mathbf{u} = 0$, where $c'(s)$ is the tangent vector $[c]_{c(s)}$. Using components, one can show that any vector that is parallel transported along c undergoes a series of infinitesimal rotations in the basis $(\mathbf{e}, \mathbf{e}^{\perp})$, leading to

$$\begin{pmatrix} u^1(s) \\ u^2(s) \end{pmatrix} = \exp\left(-J\int_0^s \omega(c'(\alpha))d\alpha\right)\begin{pmatrix} u^1(0) \\ u^2(0) \end{pmatrix}, \qquad (3)$$

where the matrix exponential $\exp(\theta J) = \cos\theta I + \sin\theta J$ is the resulting rotation matrix induced by the connection ω in order to align $T_{c(0)}M$ to $T_{c(s)}M$ (with I denoting the 2×2 identity matrix). As parallel transport along an arbitrary path involves the integral of the connection, a connection 1-form ω can be deduced from the corresponding parallel transport via differentiation [Knebelman 1951].

Curvature of connection. Any parallel-transported vector along a closed path ∂R around a simply connected region $R \subset M$ accumulates a rotation angle called the holonomy of the closed path. Given a connection 1-form ω, one can use Stokes's theorem to express the holonomy as the integral of $-d\omega$ over R, independent of the choice of the local frames. This quantity $-d\omega$ is often called the curvature K of the connection, and, in the particular case of the Levi-Civita connection, it becomes the conventional notion of (2-form) Gaussian curvature.

Geometric decomposition. Due to the linearity of the covariant derivative, the operation $\nabla\mathbf{u}$ represents a 2-tensor field on M. By denoting the reflection matrix through

$$F = \begin{pmatrix} 1 & 0 \\ 0 & -1 \end{pmatrix}$$

and omitting local bases for clarity, the matrix representation of $\nabla\mathbf{u}$ can be rearranged into *four geometrically relevant terms*:

$$\nabla\mathbf{u} = \frac{1}{2}[I\nabla\cdot\mathbf{u} + J\nabla\times\mathbf{u} + F\nabla\cdot(F\mathbf{u}) + JF\nabla\times(F\mathbf{u})], \qquad (4)$$

where $J\nabla\times\mathbf{u}$ (measuring the curl of $\mathbf{u}$) is the only antisymmetric term. Moreover, we can rewrite this decomposition as a function of two other relevant derivatives:

$$\nabla\mathbf{u} = \partial\mathbf{u} + F\bar{\partial}\mathbf{u},$$

where the holomorphic derivative $\partial \equiv \frac{1}{2}[I\nabla\cdot + J\nabla\times]$ contains divergence and curl of the vector field, neither of which depends on the choice of local frame, whereas the Cauchy-Riemann operator (or complex conjugate derivative) $\bar{\partial} \equiv \frac{1}{2}[I\nabla\cdot(F\cdot) + J\nabla\times(F\cdot)]$ depends on the choice of frame. Due to the use of reflection, $\bar{\partial}\mathbf{u}$ behaves as a 2-vector (2-RoSy) field.

Relevant energies. Based on the decomposition of the covariant derivative operator in Equation (4), we can also express the *Dirichlet energy* E_{D} of the vector field as the sum of two meaningful energies:

$$E_{\mathrm{D}}(\mathbf{u}) = \frac{1}{2}\int_M |\nabla\mathbf{u}|^2 dA = \frac{1}{2}\,(E_{\mathrm{A}}(\mathbf{u}) + E_{\mathrm{H}}(\mathbf{u})).$$

The *antiholomorphic energy* E_{A} measures how much the vector field deviates from being harmonic, and the *holomorphic energy* E_{H} measures how much the field deviates from satisfying the

Cauchy-Riemann equations:

$$\begin{cases} E_{\mathrm{A}}(\mathbf{u}) = \frac{1}{2}\int_M [(\nabla\cdot\mathbf{u})^2 + (\nabla\times\mathbf{u})^2] dA, \\ E_{\mathrm{H}}(\mathbf{u}) = \int_M (\bar{\partial}\mathbf{u})^2 dA. \end{cases}$$

As shown in Knöppel et al. [2013], the difference between E_{H} and E_{A} leads to a boundary term and a term related to the connection curvature $K = -d\omega$:

$$E_{\mathrm{A}}(\mathbf{u}) - E_{\mathrm{H}}(\mathbf{u}) = \int_{\partial M} \mathbf{u}\times(\nabla\mathbf{u})\, dA + \int_M K|\mathbf{u}|^2 dA. \qquad (5)$$

While complex numbers are often used to express these energies, we stick to basic vector calculus in our work. In the remainder of this article, all the operators and energies presented will be given a discrete formulation for their evaluation on triangle meshes.

3. ROADMAP FOR DISCRETE VECTOR FIELDS THROUGH DISCRETE CONNECTIONS

Before presenting our notion of discrete connection, we first describe the rationale upon which our formulation is based.

3.1 Of the Seeming Inadequacy of Triangle Meshes

A piecewise linear embedding of a triangulated 2-manifold in $\mathbb{R}^3$ defines piecewise constant normals per triangle and concentrates Gaussian curvature solely at vertices. As a consequence, formulating a finite-dimensional space of smooth vector fields is particularly difficult to achieve at vertices. However, since a pair of triangles can be isometrically flattened, there is a clear way to parallel transport a vector within a pair of adjacent triangles using the Levi-Civita connection induced by the Euclidean metric. A purely discrete notion of connection was derived from this idea in Crane et al. [2010] using discrete dual connection 1-forms that store rotation angles along dual edges to parallel transport a vector from one triangle to another. Discretization of divergence and curl operators were also computed based on this construction of Levi-Civita connection [Polthier and Preuß 2000; Fisher et al. 2007]. Unfortunately, these approaches do not apply to the remaining parts of the covariant derivative such as the antiholomorphic derivative in Equation (4), resulting in improper pointwise evaluations of the covariant derivative and precluding the discretization of the L_2-based energy integrals described in Section 2.4. We are therefore caught in a dilemma: either we give up on using piecewise linear surfaces and go for higher-order surface descriptions for which smoothness is no longer an issue, or we modify the canonical notion of connection on a triangle mesh by artificially "spreading" the Gaussian curvature around vertices so that one can create interpolated, *continuous* vector fields that have *finite* covariant derivatives. We opt for the second option in this article, to create a convenient numerical framework for vector field design and analysis.

3.2 Vertex-Based Discrete Vector Fields

A convenient (and common) finite-dimensional representation of vector fields on *planar* triangle meshes is through linear interpolation from one vector per vertex. Such a vertex-based discrete vector field has recently been extended to *nonflat* surface meshes and shown useful to either define local discrete first-order derivatives [Zhang et al. 2006] or evaluate global L_2 norm of derivatives [Knöppel et al. 2013]—but so far not both, as they require the explicit formulation of (necessarily nonlinear) interpolating basis functions. Additionally, the associated discrete connections in these previous approaches are not known analytically. Therefore, no analysis (in particular, of how they deviate from the canonical Levi-Civita connection of the mesh) has been proposed for this general vertex-based vector field setup. Yet, the choice of connection impacts the accuracy of differential operators and energies since it affects the evaluation of the components of the covariant derivative.

3.3 Approach & Rationale

Our work follows the discrete setup advocated in Zhang et al. [2006] and Knöppel et al. [2013] and represents tangent vector fields on triangulations as a vector $\mathbf{u}_i$ per vertex v_i, encoded intrinsically by components (u_i^1, u_i^2).

In contrast to previous work, we introduce a new definition of discrete connection that offers *closed-form basis functions for vertex-based interpolation*, thus giving explicit evaluations of these discrete vertex-based vector fields and their derivatives. In order to transition from the continuous setting to the construction of discrete connections and vector fields, we deliberately organize our presentation in Section 4 into three parts:

- First, we leverage the smooth structure of triangle meshes [Grimm and Hughes 1995] to pick charts associated with each simplex, so that the smooth notion of connection reviewed in Section 2 applies to meshes verbatim. We also identify consistency conditions that the associated transition functions satisfy and that we will preserve in the discrete realm.
- Second, we define a discretization of the notion of connection satisfying the same consistency conditions to allow for parallel transport along arbitrary paths on the triangle mesh. The resulting finite-dimensional space of finite connections is parameterized by a set of geometric parameters, and one can find within this space the (finite) connection closest to the original (Dirac-like) Levi-Civita connection.
- Last, we detail how a discrete connection can then be used to derive basis functions for the interpolation of per-vertex vectors to arbitrary points on the mesh—which then leads to closed-form expressions for both local derivatives and smoothness energies of discrete vector fields.

Our contribution can thus be interpreted as such: while piecewise linear interpolation of components does not generate continuous vector fields on nonflat meshes [Zhang et al. 2006], one can formally define a discrete notion of connection while maintaining the properties of the smooth structure of a manifold triangle mesh. We can then evaluate (and thus minimize if needed) the resulting deviation from the underlying Levi-Civita connection while guaranteeing that the first derivatives and smoothness energies of discrete vector fields remain finite.

4. CONNECTIONS ON SIMPLICIAL MANIFOLDS

We now tackle the construction of a discrete connection on simplicial manifolds.

4.1 Smooth Connections on Simplicial Charts

To motivate our discrete notion of a connection, we first describe a representation of a *smooth* connection over the triangulation $\mathcal{T}$ of a piecewise linearly embedded 2-manifold M.

Simplicial charts. We exploit the smooth structure of a discrete 2-manifold mesh by first constructing one chart for each simplex in the triangle mesh [Grimm and Hughes 1995]. Each chart is an open superset of the closure of the simplex, and the overlaps of the

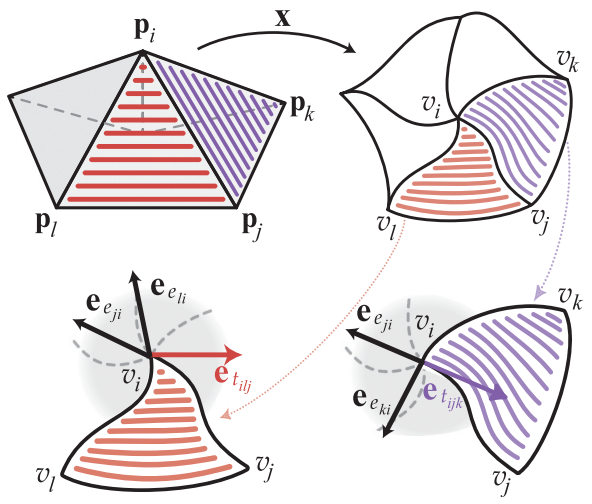

Fig. 2. **One-ring chart.** The one-ring of vertex i (top) has straight isocurves of φ_i (red) and φ_k (blue); in a chart $\mathbf{x}$ (chosen from the smooth atlas), these isocurves induce frame fields $\mathbf{e}_{t_{ilj}}$ and $\mathbf{e}_{t_{ijk}}$, respectively (bottom, only shown at v_i); the frame field in t_{ijk} (t_{ilj}, respectively) is aligned to φ_k (φ_i, respectively).

charts are defined by the adjacency relationships of the mesh. The resulting collection of charts is thus a subset of the unique maximal atlas of the manifold. We also select a metric on M that is smooth in the smooth structure of M. Note that the choice of charts and metric will not influence our construction of connection, since they are only used to identify and formulate the properties that we will make sure still hold in the discrete definition of connection.

Simplicial frames and connections. Given our charts and metric, we can now assign a local frame $(\mathbf{e}_\sigma(\mathbf{p}), \mathbf{e}_\sigma^\perp(\mathbf{p}))$ for the tangent space $T_\mathbf{p}M$ of each point $\mathbf{p}$ in a simplex σ defined on the smooth structure. For the point $\mathbf{p}$ located at vertex v_i, the frame is arbitrarily chosen from the unit vectors in $T_\mathbf{p}M$; for instance, we can select the equivalence class containing one of the emanating edges. For a point $\mathbf{p}$ on an oriented edge e_{ij}, a straightforward choice is the unit tangent vector defined by the equivalence class of the edge itself. For a point $\mathbf{p}$ in triangle t_{ijk}, it can be the unit vector defined by the equivalence class of the counterclockwise oriented isocurves of the linear basis function φ_i. Each frame field can then be extended to the rest of the associated chart (which is a superset of the simplex), but the properties for parallel transport that we will formulate will only depend on the frame field within each simplex. Notice that this construction leads to nonconstant simplicial frame fields in charts, depending on which isocurves are selected per triangle (see Figure 2). With these simplicial frame fields, one can represent a *smooth* connection 1-form by its expression ω_σ in the frame field associated with each individual simplex σ.

Simplicial transition functions. A discrete connection should allow parallel transport along an arbitrary path. Consequently, in addition to a connection 1-form within each simplex, we also need *transition functions* along the border of simplices. They consist of one function $\rho_{\sigma_1\to\sigma_2}$ for every pair of simplices σ_1 and σ_2 such that $\sigma_1 \cap \sigma_2$ is not empty. More concretely, for a point $\mathbf{p} \in \sigma_1 \cap \sigma_2$, the function $\rho_{\sigma_1\to\sigma_2}(\mathbf{p})$ is equal to the angle that $\mathbf{e}_{\sigma_1}(\mathbf{p})$ needs to be rotated by in the (continuous) tangent space $T_\mathbf{p}M$ to align with $\mathbf{e}_{\sigma_2}(\mathbf{p})$. Transition functions thus provide angles that compensate for the mismatch of frame fields, which are entirely determined by the choice of simplicial frames.

Parallel transport along a path that consists of k segments P_i in a sequence of k simplices σ_i ($i = 1, \ldots, k$, where σ_i is either a face or coface of σ_{i+1}) can then be computed as a rotation θ of the components of a vector represented in the frame field of σ_1 to obtain a vector in the frame field of σ_k, with

$$\theta = -\left(\sum_{i=1}^{k}\int_{P_i}\omega_{\sigma_i} + \sum_{i=1}^{k-1}\rho_{\sigma_i\to\sigma_{i+1}}\right),$$

where the second term accounts for the changes of simplicial frame fields at points in $\sigma_i \cap \sigma_{i+1}$. While the transition angles $\rho_{\sigma_1\to\sigma_2}$ are entirely determined by the choice of simplicial frames, independently of the connection ω being represented, they can be seen as part of the rotations involved in performing parallel transport: they are, in a way, "impulse rotations" encountered during parallel transport due to chart crossings. We thus include these rotations as part of the data required for defining parallel transport over a simplicial mesh, as described in the following definition.

Definition 7. A **smooth simplicial connection** is the description of a smooth metric connection in a given set of simplicial frames, as a continuous connection ω_σ for each $\sigma \in \mathcal{T}$ and transition angle functions $\rho_{\sigma_1\to\sigma_2}$ for each incident pair $\sigma_1, \sigma_2 \in \mathcal{T}$.

Unfortunately, the simplicial frames expressed in smooth charts do not, in general, lead to transition functions that can be described with a finite set of parameters; similarly, the smooth connection cannot be expected to have an expression with only a finite number of parameters for ω_σ. However, we can identify specific properties and consistency conditions of these transition functions and connections that we will enforce later on in Section 4.2 to ensure that our discrete notion of parallel transport is analogous to the smooth case.

PROPOSITION 1. *Given any collection of simplicial charts chosen from the smooth atlas of M, the transition angle functions* $\rho_{\sigma_1\to\sigma_2}$ *satisfy the following properties:*

$$\rho_{\sigma_1\to\sigma_2}(\mathbf{p}) = -\rho_{\sigma_2\to\sigma_1}(\mathbf{p}) \quad \forall \mathbf{p} \in \sigma_1 \cap \sigma_2;$$

$$\rho_{v_i\to e_{ij}} + \rho_{e_{ij}\to t_{ijk}}(\mathbf{p}_i) = \rho_{v_i\to t_{ijk}};$$

$$\rho_{v_i\to e_{ji}} = \pi + \rho_{v_i\to e_{ij}} + 2\pi n_{ij},$$

where n_{ij} *is an integer per edge determined by the choice of simplicial frames. Moreover, any simplicial connection satisfies*

$$\rho_{v_i\to e_{ij}} + \int_{e_{ij}}\omega_{e_{ij}} + \rho_{e_{ij}\to v_j} = \rho_{v_i\to t_{ijk}} + \int_{e_{ij}}\omega_{t_{ijk}} + \rho_{t_{ijk}\to v_j}.$$

PROOF. During parallel transport, evaluation of the transition functions happens at the intersection of incident simplices; for example, $\rho_{v\to e}$ is evaluated at vertex v, whereas $\rho_{e\to f}$ is evaluated at any point along edge e. The first property imposes that transitioning from σ_1 to σ_2 and back does not introduce any rotation. The second and fourth properties follow immediately from the alignment to an arbitrary frame on a chart covering the one-ring of v_i; such a chart exists since the manifold is compact. Moreover, these two properties will ensure that the resulting (smooth) simplicial connection does *not* have nonzero curvature on zero-area regions at vertices or around an edge, thus guaranteeing the covariant derivative to be finite everywhere. For the third equality, note that half-edges e_{ij} and e_{ji} are opposite in direction, so the values of $\rho_{v_i\to e_{ij}}$ and $\rho_{v_i\to e_{ji}}$

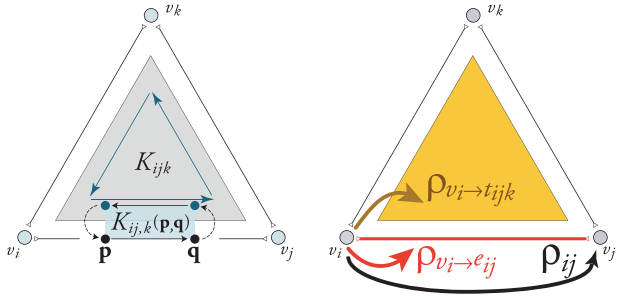

Fig. 3. **Curvature and parameters.** Left: Curvature is accumulated along a closed path around the interior of a triangle (K_{ijk}) or a closed path around a section of a half-edge ($K_{ij,k}(\mathbf{p}, \mathbf{q})$). Right: A discrete connection ρ with finite curvature ($K_{ij,k} = 0$) is encoded through only vertex-to-triangle, vertex-to-edge, and vertex-to-vertex rotation angles.

must differ by π modulo 2π. We can also evaluate $\rho_{v_i \to t_{ijk}}$ in two separate ways that must coincide:

$$\rho_{v_i \to e_{ij}} + \rho_{e_{ij} \to t_{ijk}}(\mathbf{p}_i) = \rho_{v_i \to t_{ijk}} = \rho_{v_i \to e_{ki}} + \rho_{e_{ki} \to t_{ijk}}(\mathbf{p}_i).$$

Consequently, if we denote by $\angle(\cdot, \cdot)$ the angle between two collocated tangent vectors (the metric used to evaluate the angle does not matter as this angle also appears in the other way of calculating $\rho_{v_i \to t_{ijk}}$), we have

$$\rho_{v_i \to e_{ki}} = \rho_{v_i \to e_{ij}} + \pi + \angle(e_{ij}(\mathbf{p}_i), e_{ik}(\mathbf{p}_i)) - 2\pi l_{ik},$$

where $l_{ik} = 0$ if the frame in the triangle t_{ijk} is aligned to isocurves of φ_j, and $l_{ik} = 1$ otherwise (e.g., in Figure 2, $l_{ik} = 1$ and $l_{ji} = 0$), as we may assume, without loss of generality, that we use angles between 0 and 2π for transition angles of type $\rho_{e_{ij} \to t_{ijk}}$. Thus, l_{ik} only depends on the choice of the vertex (i, j, or k) when determining the simplicial frame of t_{ijk}. Similarly, we may assume that we use angles between 0 and 2π for transition angles of type $\rho_{v_i \to e_{ij}}$. (Note that other transition angles, of type $\rho_{v_i \to e_{ji}}$ or $\rho_{e_{ji} \to t_{ijk}}$ for instance, do not have this restriction.) Thus,

$$\rho_{v_i \to e_{ik}} = \rho_{v_i \to e_{ij}} + \angle(e_{ij}(\mathbf{p}_i), e_{ik}(\mathbf{p}_i)) - 2\pi m_{ik}, \tag{6}$$

where $m_{ik} = 1$ in the only triangle t_{ijk} where $\rho_{v_i \to e_{ik}} < \rho_{v_i \to e_{ij}}$, and $m_{ik} = 0$ otherwise. Again, m_{ik} does not depend on any actual angle, but only on the counterclockwise order of e_{ji}, $\mathbf{e}_i$, and e_{ki}. We conclude that, if we define $n_{ik} \equiv m_{ik} - l_{ik}$, one must have the consistency conditions

$$\rho_{v_i \to e_{ki}} = \pi + \rho_{v_i \to e_{ik}} + 2\pi n_{ik}. \quad \square$$

4.2 Discrete Simplicial Connection

As presented earlier, a smooth simplicial connection is a description of a smooth connection in a smooth metric represented using the simplicial chart structure. To discretize this notion of simplicial connection (i.e., to form a simplicial connection with only a finite number of parameters), we need to formulate finite-dimensional representations for both the connection 1-form within each simplex and the transition angles between simplices satisfying Proposition 1. As we cover next, this can be achieved by first restricting the type of 1-form representation ω_σ to be a discrete Whitney form within each simplex σ, and then approximating the transition angle functions by linear functions, while maintaining the consistency conditions found in Proposition 1.

Whitney-based connections within simplices. Given simplicial frames, we can choose basis functions to approximate ω_σ with a

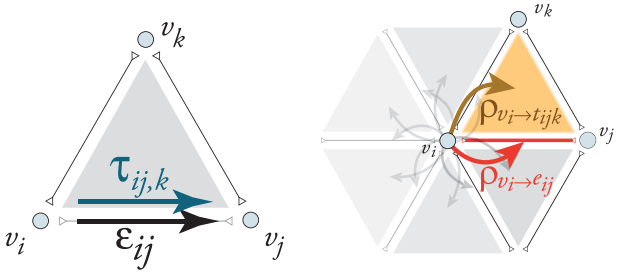

Fig. 4. **Discrete simplicial connection.** (Left) A continuous connection within simplices is encoded through edge rotation ϵ_{ij} and half-edge rotation $\tau_{ij,k}$ interpolated over edges and faces, respectively, via Whitney basis functions. (Right) Each vertex v_i is given a transition rotation angle $\rho_{v_i \to e_{ij}}$ to edge e_{ij} and $\rho_{v_i \to t_{ijk}}$ to triangle t_{ijk}.

finite number of parameters within each simplex σ. A convenient finite-dimensional representation of a connection 1-form within a simplex is to use discrete 1-forms [Desbrun et al. 2008] stored as oriented edge values interpolated via Whitney bases [Whitney 1957]. Specifically, for an oriented edge e_{ij}, we define

$$\omega_{e_{ij}} = \epsilon_{ij}\varphi_{ij} = \epsilon_{ij}[\varphi_i d\varphi_j - \varphi_j d\varphi_i] \overset{(\varphi_i + \varphi_j = 1)}{=} \epsilon_{ij} d\varphi_j,$$

where ϵ_{ij} is the total rotation angle to parallel transport along the entire edge e_{ij}. Similarly, in triangle t_{ijk}, we use

$$\omega_{t_{ijk}} = \tau_{ij,k}\varphi_{ij} + \tau_{jk,i}\varphi_{jk} + \tau_{ki,j}\varphi_{ki},$$

where $\tau_{ij,k}$ denote the accumulated angle to parallel transport inside triangle t_{ijk} along its half-edge e_{ij} (see Figure 4 (left)). Note that, due to $\varphi_{ij} = -\varphi_{ji}$, we have $\epsilon_{ij} = -\epsilon_{ji}$ and $\tau_{ji,k} = -\tau_{ij,k}$; however, $\tau_{ij,k}$ is not necessarily equal to $\tau_{ij,l}$ for the opposite triangle.

Linear transition functions. Still using the given simplicial frames, we project transition functions to a finite-dimensional representation by restricting them to linear functions within their respective simplices based on the linear basis functions φ_i. In order to ensure consistency and finite covariant derivatives, we force these transition angles to verify Proposition 1. In particular, we make use of the fourth property in Proposition 1 to impose a validity condition between transition angles $\rho_{\sigma_1 \to \sigma_2}$ and integrated connection coefficients ϵ_{ij} and $\tau_{ij,k}$:

$$\rho_{v_i \to e_{ij}} + \epsilon_{ij} + \rho_{e_{ij} \to v_j} = \rho_{v_i \to t_{ijk}} + \tau_{ij,k} + \rho_{t_{ijk} \to v_j}. \tag{7}$$

With a finite-dimensional approximation of simplicial connections and transition functions, we can now formally construct (and thus, define) a discrete connection on simplicial meshes, given a set of simplicial frames.

Definition 8. A **discrete simplicial connection** is a set of transition angles $\rho_{\sigma_1 \to \sigma_2}$ and a set of Whitney-based connections ϵ per edge and τ per triangle, such that the four properties in Proposition 1 are satisfied, and the transition functions from edges to triangles are linear in the hat functions φ_i.

Reduced connection parameters. We now analyze the properties in Proposition 1 in more detail and show that the previous definition of discrete simplicial connection can be constructed from a reduced set of parameters. To this end, we introduce a new parameter, ρ_{ij}, which indicates the rotation angle accumulated during a parallel transport from v_i to v_j along edge e_{ij}.

PROPOSITION 2. *A discrete simplicial connection can be fully determined by the following reduced set of parameters in a given set of simplicial frames:*

- $3|F|$ *vertex-to-triangle transition rotations* $\rho_{v_i \to t_{ijk}}$,
- $2|E|$ *vertex-to-edge transition rotations* $\rho_{v_i \to e_{ij}}$, *and*
- $|E|$ *vertex-to-vertex rotations* ρ_{ij}.

For clarity, we denote by ρ *the collection of these parameters, that is,* $\rho = (\{\rho_{ij}\}, \{\rho_{v_i \to e_{ij}}\}, \{\rho_{v_i \to t_{ijk}}\})$ *(see Figure 3 (right)).*

PROOF. We begin by noting that the transition $\rho_{\sigma_1 \to \sigma_2}$ for the case $\sigma_2 \subset \sigma_1$ can be calculated as $-\rho_{\sigma_2 \to \sigma_1}$ if we only construct the angles from a simplex to a coface, automatically satisfying the first property of Proposition 1. Next, we leverage the fact that Equation (7) (or, equivalently, the fourth property in Proposition 1) equates the angle incurred during the transport along a single edge to deduce how the connection discrete 1-form coefficients depend on the variables ρ_{ij}:

$$\begin{aligned} \epsilon_{ij} &= -\rho_{v_i \to e_{ij}} + \rho_{ij} + \rho_{v_j \to e_{ij}}, \\ \tau_{ij,k} &= -\rho_{v_i \to t_{ijk}} + \rho_{ij} + \rho_{v_j \to t_{ijk}}. \end{aligned} \tag{8}$$

Because of the second equation in Proposition 1 and of the linearity requirement, we also observe that the rotation angle $\rho_{e_{ij} \to t_{ijk}}$ at a point $\mathbf{p} \in e_{ij}$ between the edge e_{ij} and an incident triangle t_{ijk} can be expressed as

$$\begin{aligned} \rho_{e_{ij} \to t_{ijk}}(\mathbf{p}) = \varphi_i(\mathbf{p})\,(\rho_{v_i \to t_{ijk}} - \rho_{v_i \to e_{ij}}) \\ + \varphi_j(\mathbf{p})\,(\rho_{v_j \to t_{ijk}} - \rho_{v_j \to e_{ij}}). \end{aligned} \tag{9}$$

At last, using the third property in Proposition 1, one can show that $\rho_{ij} = -\rho_{ji} + 2\pi(n_{ij} - n_{ji})$, where n_{ij} is a constant integer determined by the choice of simplicial frames. Thus, we only need one ρ_{ij} per edge to define a discrete simplicial connection entirely. □

Discrete curvature. Equipped with reduced parameters, the curvature of a discrete simplicial connection in a triangle's interior becomes solely determined by ρ_{ij} via the following expression:

$$-K_{ijk} = \rho_{ij} + \rho_{jk} + \rho_{ki}.$$

We have thus locally spread the Gaussian curvature of the original mesh to make our notion of simplicial connections both finite-dimensional and finite—unlike the canonical connection of the triangle mesh. This is the price to pay to have continuity of the resulting notion of discrete vector fields as we detail next. We will see later on in Section 5.3 that the deviation generated by our discretization with respect to the original Levi-Civita connection can be easily quantified—and thus, minimized if needed.

4.3 Discrete Vector Fields

So far we have presented a finite-dimensional definition of connection on simplicial meshes. However, simplicial frame fields and related tangent vectors are expressed pointwise via charts within simplices. In this section, we propose a definition of a finite-dimensional representation for vector fields that is compatible to the notion of discrete simplicial connection. As we will show, this construction leads to analytical basis functions for interpolation of frame and vector fields to arbitrary points on a triangulation, where the charts are parameterized through barycentric coordinates.

Vertex-based vector fields. Similar to the work of Zhang et al. [2006] and Knöppel et al. [2013], we propose to encode discrete vector fields using only vertices: given a frame per vertex v_i, a discrete vector $\mathbf{u}_i$ at v_i is represented by coordinates u_i^1 and u_i^2. In contrast to previous work, we now have a well-defined notion of parallel transport within any simplex of the triangulation determined by our discrete simplicial connection ρ. This allows us to parallel transport vertex-based vectors to any point inside edges and triangles.

Construction of analytical basis functions. Given a discrete connection ρ, we define a basis function Ψ_i per vertex v_i. Its expression $\Psi_i|_t$ within each incident triangle t is constructed by first using the rotation $-\rho_{v_i \to t}$ to convert the vector $\mathbf{u}_i$ stored in the local frame $\mathbf{e}_{v_i}$ of v_i to its coordinates in $\mathbf{e}_t$ (the local frame of the incident triangle t) at the *same* point; we then parallel transport the resulting vector expressed in the frame $\mathbf{e}_t$ along a straight path from v_i to an arbitrary point $\mathbf{p}$ in t under the connection 1-form ω_t, which defines a local frame field

$$\Phi_i|_t(\mathbf{p}) = \left(\mathbf{e}_t, \mathbf{e}_t^{\perp}\right) \exp\left[-J\left(\rho_{v_i \to t} + \int_{v_i \to \mathbf{p}} \omega_t\right)\right].$$

With these local frame fields, we make use of the scalar basis functions φ_i at $\mathbf{p}$ to blend the parallel transported vectors from each corner of the triangle. Since our connection ω_t is linear within each triangle, the resulting basis function for a vertex v_i is easily expressed in closed form as

$$\begin{aligned} \Psi_i\Big|_{t_{ijk}}(\mathbf{p}) &= \varphi_i(\mathbf{p})\Phi_i\Big|_{t_{ijk}}(\mathbf{p}) \\ &= \varphi_i(\mathbf{p})\left(\mathbf{e}_{t_{ijk}}, \mathbf{e}_{t_{ijk}}^{\perp}\right) \\ &\qquad \exp\left[-J(\rho_{v_i \to t_{ijk}} + \tau_{ij,k}\varphi_j(\mathbf{p}) + \tau_{ik,j}\varphi_k(\mathbf{p}))\right]. \end{aligned}$$

The interpolated vector field $\mathbf{u}$ at a point $\mathbf{p}$ can then be evaluated anywhere on the mesh via

$$\mathbf{u}(\mathbf{p}) = \sum_i \Psi_i(\mathbf{p}) \begin{pmatrix} u_i^1 \\ u_i^2 \end{pmatrix}.$$

Note that this interpolation is visually quite similar to a linear interpolation for a discrete as-Levi-Civita-as-possible connection, but can be dramatically different for other connections. For example, the inset shows a vector (in green) locally interpolated by a basis Ψ_i over a non-flat one-ring for two choices of connection: an as-Levi-Civita-as-possible connection (*top*) versus the same connection for which one of the vertex-to-face angles has been doubled (*bottom*).

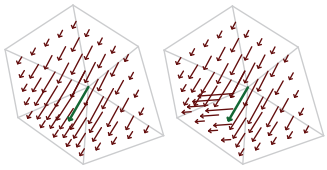

4.4 Discussion

As we will demonstrate in Section 6, one can easily compute the differential operators and energies associated with our finite-dimensional space of vector fields. However, most geometry processing tools assume the Levi-Civita connection induced by the Euclidean embedding, which *cannot* be encoded by a discrete simplicial connection: as we discussed earlier, the connection is zero within each simplex, and only the edge-to-triangle transition angle $\bar{\rho}_{e_{ij} \to t_{ijk}}$ is well defined and constant along each edge e_{ij} as

$$\forall \mathbf{p} \in e_{ij},\ \ \bar{\rho}_{e_{ij} \to t_{ijk}}(\mathbf{p}) = \angle(\mathbf{e}_{e_{ij}}, \mathbf{e}_{t_{ijk}}), \tag{10}$$

where the angle is measured in the Euclidean-induced metric. Our construction, instead, purposely offers a connection that defines a continuous covariant derivative on simplicial meshes. Therefore, we describe next how to define a discrete connection *as close as*

possible to the original Levi-Civita connection of the mesh while keeping the associated notion of covariant derivative finite.

5. COMPUTING DISCRETE CONNECTIONS

The parameters of our formulation of connections over triangulated manifolds need to be determined to create an instance of discrete connection. We first provide local choices of parameters that were implicit in previous work, before introducing a global optimization procedure that mimics the work of Crane et al. [2010] but within our (vertex-based) connection setup, in the sense that it makes the discrete simplicial connection as close as possible to the canonical Levi-Civita connection of the input surface.

5.1 Connection Derived from Geodesic Polar Maps

One initial choice for evaluating ρ is based on the geodesic polar map. We first evaluate $\rho_{v\to e}$ from rescaled tip angles, then derive ρ_{ij} solely from $\rho_{v\to e}$, and finally propose a set of $\rho_{v\to t}$ to provide a complete assignment for ρ. The evaluation of ρ_{ij} is consistent with both Zhang et al. [2006] and Knöppel et al. [2013]. However, Zhang et al. [2006] construct a connection via parallel transports along geodesic lines from vertices, rendering the covariant derivatives there infinite since $\rho_{v\to t}$ is different for the same pair of v and t depending on which geodesic line the nearby point is on. Instead, Knöppel et al. [2013] does not provide a set of $\rho_{v\to t}$, and thus does not have closed-form formulae to evaluate covariant derivatives pointwise.

The geodesic polar map proportionally rescales tip angles around each vertex such that they sum to 2π, inducing a flattening of the immediate surroundings of each vertex v_i through a scaling factor

$$s_i = 2\pi / \sum_{t_{ijk}} \theta_{kij} \equiv 2\pi/(2\pi - \kappa_i), \tag{11}$$

where κ_i is the commonly used discrete Gaussian curvature integral for v_i. These parameterization charts are not necessarily charts in the atlas of smooth charts, as the transition functions between overlapping geodesic polar maps of two adjacent vertices are not smooth in general. However, they suggest a way to evaluate the transition angles $\rho_{v\to e}$. Without loss of generality, one of the edge directions can be chosen as the frame at vertex v_i; using Equation (6), we can then evaluate $\rho_{v_i\to e_{ik}} = \rho_{v_i\to e_{ij}} + \angle(e_{ij}, e_{ik})$, where $\angle(e_{ij}, e_{ik}) = s_i \angle(\mathbf{e}_{ij}, \mathbf{e}_{ik}) = s_i\theta_{kij}$ is the angle in the intrinsic tangent plane spanned by geodesic lines through the vertex under the geodesic polar map. The vertex-to-vertex coefficient ρ_{ij} of the discrete connection is then set to be

$$\rho_{ij} = \rho_{v_i\to e_{ij}} - \rho_{v_j\to e_{ij}},$$

which is equivalent to setting $\epsilon_{ij} = 0$. The triangle curvature K_{ijk} of the connection finally becomes

$$K_{ijk} = (s_i - 1)\theta_{kij} + (s_j - 1)\theta_{ijk} + (s_k - 1)\theta_{jki}.$$

This is precisely the choice that Knöppel et al. [2013] made—except that their restriction on the range of the Gaussian curvature is unnecessary with our integers n_{ij} determined by the choice on simplicial frames.

This choice of vertex-to-vertex rotation angles does not, however, fully determine a discrete connection—although it is enough to evaluate the Dirichlet energy of a vector field as we will see in Section 6. Indeed, transition angles from vertices to triangles $\rho_{v\to t}$ are crucial for the local evaluation of the first-order derivatives' divergence, curl, and $\bar{\partial}$. An intuitive choice for these vertex-to-triangle rotations is to use the vertex-to-edge transition rotations, the vertex-to-vertex coefficients, and the well-defined angles (measured in the actual Euclidean metric) from the edge frame to the triangle frame:

$$\rho_{v_i\to t_{ijk}} = \rho_{v_i\to e_{ij}} + \bar{\rho}_{e_{ij}\to t_{ijk}},$$

where the Levi-Civita connection $\bar{\rho}_{e_{ij}\to t_{ijk}}$ of Equation (10) is used. However, this choice is biased since it only considers the transition rotations of e_{ij} and not of its neighboring edges. To be consistent with the geodesic polar map, the rotation from the vertex frame basis $\mathbf{e}_{v_i}$ to any direction between e_{ij} and e_{ik} should be directly computed based on the scaling factor s_i and should result in a rotation angle in between $\rho_{v_i\to e_{ij}}$ and $\rho_{v_i\to e_{ik}}$. One of the many different ways to enforce this property is thus to pick an arbitrary interior point $\mathbf{c}_{ijk}$ (such as the in-center or the barycenter) of each triangle t_{ijk}, to define $\rho_{v_i\to\mathbf{c}_{ijk}} = (\rho_{v_i\to e_{ij}} + \rho_{v_i\to e_{ik}} + 2\pi n_{ik})/2$, and then to define the vertex-to-triangle transition rotations as

$$\rho_{v_i\to t_{ijk}} = \rho_{v_i\to\mathbf{c}_{ijk}} + \angle(\mathbf{c}_{ijk} - \mathbf{p}_i, \mathbf{e}_{t_{ijk}}), \tag{12}$$

where, again, the angles $\angle$ are measured in the actual Euclidean metric of the input mesh.

5.2 Locally Optimal Connection 1-Form

The choice of geodesic polar map may, however, result in large connection values ω_t (as deduced from ρ through Equation (8)), indicating a significant mismatch between the local original Levi-Civita connection (which is $\mathbf{0}$ inside a triangle) and its discrete counterpart. A simple improvement can be achieved by choosing the vertex-to-triangle rotations $\rho_{v\to t}$ that minimize the L_2 norm of this deviation within each triangle while keeping the vertex-to-vertex coefficients ρ_{ij} unchanged. As the L_2 norm of ω_t per triangle is a quadratic function of its edge values $\tau_{ij,k}$, $\tau_{jk,i}$, and $\tau_{ki,j}$ using the mass matrix of Whitney 1-form bases, the local optimal values are found in closed form to be simply $\tau_{ij,k} = -K_{ijk}/3$, which leads to

$$\int_{t_{ijk}} \omega_{t_{ijk}} \wedge \star\omega_{t_{ijk}} = \frac{1}{36}(\cot(\theta_{ijk}) + \cot(\theta_{jki}) + \cot(\theta_{kij}))K_{ijk}^2.$$

There are, however, multiple choices of vertex-to-triangle rotations that achieve this locally minimal connection. For instance, we could pick one arbitrary transition angle $\rho_{v_i\to t_{ijk}}$ per triangle t_{ijk}, then find $\rho_{v_j\to t_{ijk}}$ and $\rho_{v_k\to t_{ijk}}$ so that, for $q \in \{j, k\}$,

$$\rho_{v_q\to t_{ijk}} = \rho_{v_i\to t_{ijk}} + \rho_{qi} + \tau_{iq}. \tag{13}$$

One can, instead, compute the three triplets of vertex-to-triangle transition angles induced by fixing each one of the corner transition angles individually using Equation (13) and average their values to avoid bias. This averaged choice leads to better accuracy in singularity direction control (see Section 7) and has proven to be, in all our tests, the *local* definition of connection that generates the least amount of numerical errors (see Table I).

5.3 As-Levi-Civita-As-Possible Connection 1-Form

Deriving a discrete connection through a geodesic polar map as in Knöppel et al. [2013] leads to reasonable connection 1-forms ρ_{ij} and $\rho_{v\to e}$ on primal edges, and local optimizations of $\rho_{v\to t}$ further minimize the resulting triangle-based connection 1-form. We can, however, directly compute a *globally* optimal discrete connection by computing the parameters ρ_{ij}, $\rho_{v\to e}$, and $\rho_{v\to t}$ that minimize the deviation between the resulting connection ρ and the actual canonical Levi-Civita connection $\bar{\rho}_{e\to t}$ (Equation (10)) of the piecewise flat mesh. In order to define a meaningful notion of optimal connection, we propose the following two area-integrated measurements

of deviation:

$$D_T(\rho) = \sum_t \int_t \omega_t \wedge \omega_t,$$
$$D_E(\rho) = \sum_{e,t \mid e \subset t} w_{e,t} \int_e (\rho_{e\to t}(\mathbf{p}) - \bar{\rho}_{e\to t})^2 dl,$$

where $\rho_{e\to t}(\mathbf{p})$ is the linearly varying transition angle function given in Equation (9), and $w_{e_{ij},t_{ijk}} = \tan\theta_{jki}$ is the inverse of the cotan weight for the Hodge star of 1-forms within the triangle (for tip angles greater than or equal to $\pi/2$, we can use a fixed large value for $w_{e,t}$ instead without substantial impact on the resulting coefficients, since the effect of the cotan weights on the global result is minor as noticed in Crane et al. [2010] for the dual version). D_T measures the deviation from the flat connection within triangles, while D_E measures the difference between the true Levi-Civita connection measured by the angles $\angle$ on the input mesh and the transition angles induced by the reduced parameters of ρ. Minimizing the quadratic total deviation $D_T + D_E$ is thus simple: the optimization procedure amounts to solving a linear system in ρ after we fix its kernel of size $|V|$ by setting to zero one of the vertex-to-face transition angles $\rho_{v_i\to t_{ijk}}$ per vertex v_i (these $|V|$ gauge values do not affect the result, as they amount to a rotation angle of the arbitrary frame direction $\mathbf{e}_{v_i}$). Both energies are expressed as quadratic functions of ρ; note that the integrated deviation D_E does not depend on ρ_{ij} since the contributions from ω_t and ω_e cancel out along each edge.

5.4 Trivial Connections

We just described how our definition of a discrete connection can be made as close as possible to the Levi-Civita connection $\bar{\rho}$ through a linear solve. In fact, we can also create a connection as close as possible to *any* metric connection with arbitrary cone singularities at vertices, similar to the *trivial connections* of Crane et al. [2010]: in our context, trivial connections are created by using angles $\tilde{\rho}_{e_{ij}\to t_{ijk}} = \bar{\rho}_{e_{ij}\to t_{ijk}} + \alpha_{ij,k}$, where $\alpha_{ij,k}$ is an adjustment angle, and the cone singularity at v_i has a connection curvature

$$K_i = \sum_{t_{ijk}} (\rho_{v_i\to e_{ij}} + \tilde{\rho}_{e_{ij}\to t_{ijk}} - \tilde{\rho}_{e_{ki}\to t_{ijk}} - \rho_{v_i\to e_{ki}}).$$

If the adjustment angles have been picked such that $K_i = 0$ for all vertices that are not one of the selected singularities, and if we replace $\bar{\rho}_{e\to t}$ in the deviation D_E by $\tilde{\rho}_{e\to t}$, our optimization will find the closest discrete simplicial connection to this trivial connection, thus extending the method of Crane et al. [2010] to our primal setup. As we will demonstrate in Section 8, our optimization of the discrete connection improves the accuracy of all further numerical evaluations. More importantly, we can now formulate in closed-form pointwise or locally integrated derivatives *and* their L_2 norms as explained next.

6. CONNECTION-BASED OPERATORS

Equipped with a discrete simplicial connection ρ (Section 4.2) and an interpolation basis function Ψ_i per vertex v_i (Section 4.3), we now derive an exact expression for any first-order differential operator or energy of a vertex-based vector field.

6.1 Discrete Covariant Derivative

We start by computing the gradient of our nonlinear basis function Ψ_i. Dropping the basis $(\mathbf{e}_t, \mathbf{e}_t^\perp)$ for clarity, the covariant derivative of our basis functions within triangle t_{ijk} is formally derived via

$$\begin{aligned}
\nabla\Psi_i &= \nabla(\varphi_i\Phi_i) = \Phi_i \otimes d\varphi_i + \varphi_i \nabla\Phi_i \\
&= \Phi_i \otimes d\varphi_i + J\Psi_i \otimes (\omega_t - \tau_{ij,k} d\varphi_j - \tau_{ik,j} d\varphi_k) \\
&= \Phi_i \otimes d\varphi_i + J\Psi_i \otimes \\
&\quad (\omega_t + \tau_{ij,k}(\varphi_{jk} - \varphi_{ij}) + \tau_{ik,j}(\varphi_{ki} - \varphi_{jk})) \\
&= \Phi_i \otimes d\varphi_i - K_{ijk} J\Psi_i \otimes \varphi_{jk}.
\end{aligned}$$

6.2 Discrete Energies

The discretization of the smoothness energies E_D, E_A, and E_H introduced in Section 2.4 requires the pairing of our basis functions Ψ and their gradients $\nabla\Psi$. This leads to a mass matrix M and a stiffness matrix K with entries of the form

$$M_{ij} = \int_{\mathcal{T}} \Psi_i \cdot \Psi_j, \qquad K_{ij} = \int_{\mathcal{T}} \nabla\Psi_i : \nabla\Psi_j.$$

Note that, while the basis functions Ψ_i depend on the choice of vertex-to-triangle transition rotations $\rho_{v\to t}$, one can algebraically show that the integrant in M_{ij} (K_{ij}, respectively) does not depend on vertex-to-triangle transition rotations, for example:

$$\Psi_i(\mathbf{p}) \cdot \Psi_j(\mathbf{p}) = \varphi_i(\mathbf{p})\varphi_j(\mathbf{p}) \exp[J(K_{ijk}\varphi_k(\mathbf{p}) + \rho_{ij})].$$

Consequently, our discrete energies reduce to expressions similar to the result of Knöppel et al. [2013], except that we use an optimized connection ρ instead of the vertex-to-vertex coefficients derived from the geodesic polar map (Section 5.1). The rotations $\rho_{v\to t}$ are, however, crucial for the evaluation of pointwise or integrated first-order derivatives, as we discuss next.

6.3 Discrete First-Order Derivatives

To derive the integrals of first-order operators per triangle t_{ijk}, it is convenient to choose a barycentric-coordinate parameterization $(x(\mathbf{p}), y(\mathbf{p})) = (\varphi_j(\mathbf{p}), \varphi_k(\mathbf{p}))$ in t_{ijk}, for which the metric is

$$g = \begin{pmatrix} \mathbf{e}_{ij}\cdot\mathbf{e}_{ij} & \mathbf{e}_{ij}\cdot\mathbf{e}_{ik} \\ \mathbf{e}_{ij}\cdot\mathbf{e}_{ik} & \mathbf{e}_{ik}\cdot\mathbf{e}_{ik} \end{pmatrix}.$$

The components of $\nabla\Psi_i$ can now be evaluated given any constant frame field $(\mathbf{e}_1, \mathbf{e}_2)$ within the triangle. For instance, if one picks $\mathbf{e}_1 = \frac{1}{g_{11}}\frac{\partial}{\partial x}$, one gets inside triangle t_{ijk}:

$$\begin{aligned}
\nabla_{\mathbf{e}_1}\Psi_i &= \Phi_i d\varphi_i(\mathbf{e}_1) - K_{ijk}\varphi_i J\Phi_i(\varphi_j d\varphi_k - \varphi_k d\varphi_j)(\mathbf{e}_1) \\
&= \frac{1}{g_{11}}\left(dx\left(\frac{\partial}{\partial x}\right) - K_{ijk} x J(-y d(x+y))\left(\frac{\partial}{\partial x}\right)\right)\Phi_i \\
&= \frac{1}{g_{11}}(I + K_{ijk} xy J)\Phi_i.
\end{aligned}$$

The four operators involved in Equation (4) are then assembled via

$$\text{div}\ \Psi_i = \mathbf{e}_1 \cdot \nabla_{\mathbf{e}_1}\Psi_i + \mathbf{e}_2 \cdot \nabla_{\mathbf{e}_2}\Psi_i,$$

$$\text{curl}\ \Psi_i = \mathbf{e}_1 \cdot \nabla_{\mathbf{e}_2}\Psi_i - \mathbf{e}_2 \cdot \nabla_{\mathbf{e}_1}\Psi_i,$$

$$\overline{\text{div}}\ \Psi_i = \mathbf{e}_1 \cdot \nabla_{\mathbf{e}_1}\Psi_i - \mathbf{e}_2 \cdot \nabla_{\mathbf{e}_2}\Psi_i,$$

$$\overline{\text{curl}}\ \Psi_i = \mathbf{e}_1 \cdot \nabla_{\mathbf{e}_2}\Psi_i + \mathbf{e}_2 \cdot \nabla_{\mathbf{e}_1}\Psi_i.$$

Note that, as expected, a rotation by θ in the triangle's local frame produces no change in div or curl, but it results in a rotation $\exp(J2\theta)$ of the Cauchy-Riemann operator $\bar{\partial} = 1/2(\overline{\text{div}}, \overline{\text{curl}})$. If,

on the other hand, the connection from a vertex v to an incident triangle t is changed by an angle θ, it results in a redistribution of the four terms $(\mathrm{div}_{\mathrm{new}}, \mathrm{curl}_{\mathrm{new}})^T = \exp(J\theta)(\mathrm{div}, \mathrm{curl})^T$ and $\bar{\partial}_{\mathrm{new}} = \exp(J\theta)\bar{\partial}$, but their combined L_2-norms (E_A and E_H) remain unchanged.

Triangle-based integrals. The discrete versions of these operators are defined as their continuous integrals over triangles as it provides numerically robust local averages:

$$\mathrm{div}_t\ \Psi_i = \int_t \mathrm{div}\,\Psi_i, \quad \mathrm{curl}_t\ \Psi_i = \int_t \mathrm{curl}\,\Psi_i, \quad \bar{\partial}_t \Psi_i = \int_t \bar{\partial}\Psi_i.$$

The integration can be done in closed form since it essentially involves terms such as $x\exp(Jx)$. For numerical evaluation, Chebyshev expansion is recommended [Knöppel et al. 2013] to handle the expressions when the connection curvature is either small or large. However, with our optimized connection, it is safe to assume that the curvature is small enough to use a simpler Taylor expansion, with essentially the same accuracy. While the integral of our discrete connections on local half-edge cycles (Figure 3) is zero by design, the total integral of the discrete operators we just formed does not necessarily vanish as it should: the triangle integral of divergence reduces to the boundary integral formed by half-edges considered as part of the triangle, which therefore do not account for the edge integrals. Thus, Stokes's theorem for divergence and curl will not hold when we sum triangle integrals. In fact, this discrepancy between integrals along the boundary of triangles versus edges is only one of the two sources of inaccuracy: the other source is the deviation of the connection 1-form ω from the (trivial) Levi-Civita connection within each triangle. It bears noticing that our optimization target function in Section 5.3 is precisely a measure of these two discrepancies. Thus, our optimized discrete connections lead to higher-quality first-order derivative operators than those induced by the geodesic polar map. The final expressions of our discrete operators are analytically found through symbolic integration (see Appendix A.3).

Edge-based integrals. If a precise enforcement of Stokes's theorem is required, the per-triangle integral evaluation of first-order derivatives can be defined via boundary integrals instead: using our edge-based connection ω_e, we can define another set of discrete operators, defined on each triangle as

$$\mathrm{div}_t\ \Psi_i = \int_{\partial t} \Psi_i \times d\mathbf{l}, \quad \mathrm{curl}_t\ \Psi_i = \int_{\partial t} \Psi_i \cdot d\mathbf{l},$$

where the basis function Ψ is expressed along the edge as

$$\Psi_i|_{e_{ij}}(\mathbf{p}) = \varphi_i(\mathbf{p})\exp[-J(\epsilon_{ij}\varphi_j(\mathbf{p}) + \rho_{v_i \to e})].$$

The Cauchy-Riemann operator is defined in a similar fashion via

$$\bar{\partial}_t \Psi_i = \frac{1}{2}\int_{\partial t} ((F\Psi_i) \times d\mathbf{l}, (F\Psi_i) \cdot d\mathbf{l})^T,$$

where the reflection F is done w.r.t. the frame $\mathbf{e}_t$ in triangle t. The closed-form expressions of these discrete operators are given in Appendix A.2. Both triangle-based and edge-based discrete approaches to evaluating local integrals of first-order derivatives exhibit similar numerical accuracy, as we will discuss in Section 8.

7. VECTOR AND N-DIRECTION FIELD DESIGN

The operators and energies we have defined based on our discrete connection are well suited to the design of visually smooth vector fields on triangle meshes through basic linear algebra, as one has control over the behavior of their singularities (both position *and* orientation) as well as their alignment. In this section, we present two different approaches to vector field design that build upon and extend previous work through the use of our discrete connections and covariant derivatives. Note that creating a smooth n-vector or n-direction field is also a trivial matter: the exact same vector field design procedure can be used first in a connection where all angles have been multiplied by n, and the resulting vector field is converted to an n-vector field by dividing the angle the vector field makes with each vertex reference direction $\mathbf{e}_{v_i}$ by n (see Figure 5). We can then normalize the resulting n-vector field to make it an n-direction field as proposed in Knöppel et al. [2013].

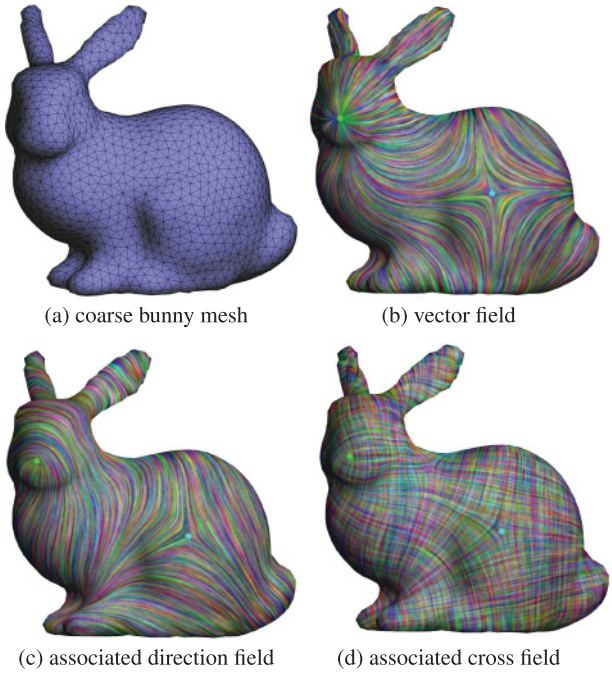

(a) coarse bunny mesh (b) vector field (c) associated direction field (d) associated cross field

Fig. 5. **From vector field to n-vector fields.** A discrete vector field, even on a coarse mesh, can be directly converted into an n-vector or n-direction field by scaling the connection angles. Here, a bunny mesh (a) and a vector field with a source and a saddle on one side (b) are converted into a 2-RoSy (direction) field (c) and a 4-RoSy (cross) field (d).

It should be noted here, as it will become important in the course of this section, that for an n-vector field $\mathbf{u}$ with $n \geq 2$, the notions of divergence and curl become dependent on the choice of frame: they now represent the components of an $(n-1)$-vector field $\partial\mathbf{u}$ as we demonstrate in Appendix A. Conversely, the reflected divergence and reflected curl represent an $(n+1)$-vector field $\bar{\partial}\mathbf{u}$.

7.1 Variational Approach

The overall procedure of our first approach to design a vector field is based on a quadratic minimization driven by user-specified constraints, extending the approach of Fisher et al. [2007]. From a globally optimized discrete connection, we define a penalty energy P for a vector field $\mathbf{u}$ as

$$P(\mathbf{u}) = \tfrac{1}{2}\int_{\mathcal{T}} (\mathrm{div}\,\mathbf{u} - d)^2 + (\mathrm{curl}\,\mathbf{u} - c)^2 + (\bar{\partial}\mathbf{u} - \mathbf{s})^2 + w(\mathbf{u} - \mathbf{u}_0)^2,$$

where d prescribes sources/sinks, c controls vortices, $\mathbf{s}$ controls the antiholomorphic derivative of the field (and thus, the desired saddle

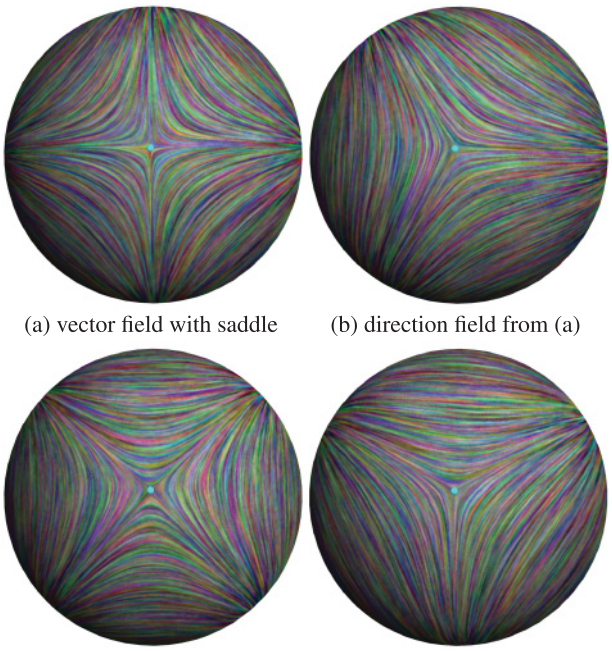

(a) vector field with saddle (b) direction field from (a)

(c) $\frac{\pi}{4}$-rotation of saddle in (a) (d) direction field from (c)

Fig. 6. **Orientation control for negative index singularities.** From a vector field (a) on a sphere with a saddle point with index -1 (its corresponding 2-RoSy field (b) forming a trisector of index $-1/2$, respectively), the user can directly control the orientation (c) of the saddle (the orientation of the trisector (d), respectively) without affecting its position on the surface.

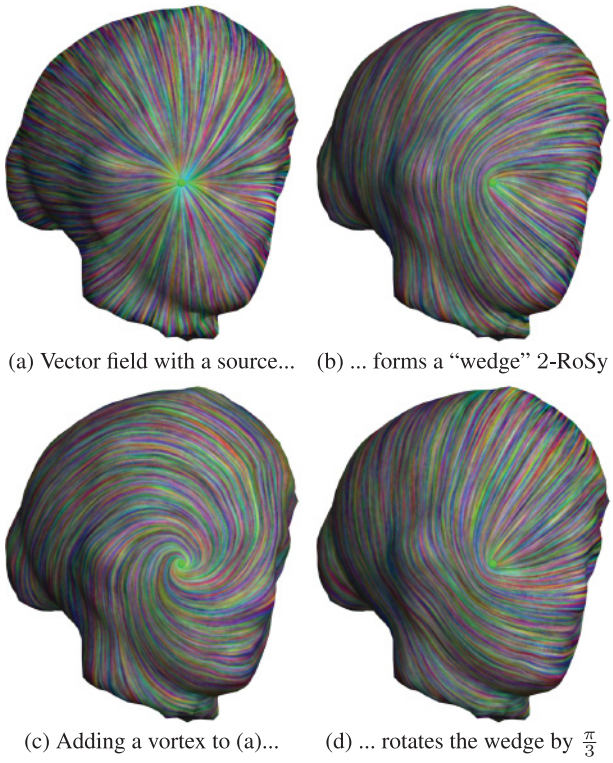

(a) Vector field with a source... (b) ... forms a "wedge" 2-RoSy

(c) Adding a vortex to (a)... (d) ... rotates the wedge by $\frac{\pi}{3}$

Fig. 7. **Orientation control of positive index singularities.** By setting a divergence/curl pair $(1, 0)$ on a triangle, a source (singularity of index 1) is formed in the vector field (a wedge singularity of index $1/2$ on the associated 2-RoSy field, respectively). Changing this pair to $(\cos(\frac{\pi}{3}), \sin(\frac{\pi}{3}))$, a vortex (c) is added to the source (creating log-spiraling streamlines) while the corresponding orientation field (d) has its wedge rotated by $\pi/3$.

points), $\mathbf{u}_0$ is a guidance vector field, and w is a weight used for local or global alignment constraints. The integration of this quadratic energy can be done on a per-triangle basis, which reduces to a Poisson-like linear system $A\mathbf{U} = b$ for a matrix $A = -2\Delta_\omega + wI$, where Δ_ω can be seen as the discrete version of the connection Laplacian (which handles boundary conditions naturally, unlike the deRham Laplacian used in Fisher et al. [2007]). This matrix A has the exact same structure as the one in Knöppel et al. [2013], except that we use our optimized ρ_{ij} instead of vertex-to-vertex rotations induced by the geodesic polar map. The right-hand-side term b relies on the discrete divergence, curl, and Cauchy-Riemann operators, which use our optimized vertex-to-triangles coefficients as well—this term is an extension of the work of Liu et al. [2013] for nonflat domains. While we will not explore this possibility here, note that the user can also start from a chosen trivial connection (see Section 5.3) instead of the Levi-Civita connection for even greater flexibility in editing.

Controlling singularity orientation. Using our penalty energy P, we can control the orientation of positive index singularities, including vortices, sources/sinks, and combinations thereof. This was already possible in the divergence- and curl-based approach of Fisher et al. [2007]. With our Cauchy-Riemann operator, we can *also* control negative index singularities (i.e., saddle points, see Figure 6) and their direction, which was impossible in previous work.

Positively indexed singularities can be constructed by assigning pairs of nonzero values (d_{ijk}, c_{ijk}) on selected triangles (and zero for all others) representing the local divergence and curl that the user desires. Note that the ratio c/d controls the direction of singularities for n-vector fields: while the shape of an index-1 singularity in a vector field is invariant under rotation, changing a pair (d_{ijk}, c_{ijk}) to $\exp(J\theta)(d_{ijk}, c_{ijk})$ when editing an index-$1/n$ singularity in an n-vector field results in a rotation of $\theta/(n-1)$ of the singularity (see Figure 7).

In order to control saddle points, one can assign prescribed values $\mathbf{s}_{ijk}$ of the antiholomorphic derivative of the vector field at selected triangles. The ratio between the two components of $\mathbf{s}_{ijk}$ in a triangle then indicates the angle that the symmetry axis of the saddle point makes with the simplicial frame field $\mathbf{e}_{t_{ijk}}$. In this case, $\bar{\partial}\mathbf{u}$ is, itself, a 2-vector field, so rotating the saddle point by $\theta/2$ amounts to using $\exp(J\theta)\mathbf{s}_{ijk}$. For $-1/n$-singularities in n-direction fields, we will get $\theta/(n+1)$ rotations instead. Figure 6 shows an example where a saddle point is rotated by $\pi/3$ by changing the components of $\mathbf{s}_{ijk}$ on the triangle t_{ijk} containing the saddle.

Constraining alignment. Vector or n-direction fields can also be modified via alignment constraints, either via an input direction field or via user-drawn strokes. If we are given a target n-vector or n-direction field represented by $\mathbf{u}_0$, we balance the smoothness (and singularity control if needed) and the alignment term via a user-specified weight w as indicated in the last term of energy P. For more local editing, the user can draw strokes on the mesh as an intuitive way to provide control over the design. We can essentially follow the approach of Fisher et al. [2007] to create a locally supported vector field $\mathbf{u}_0$ and enforce it via the same penalty term used earlier. See an example in Figure 8.

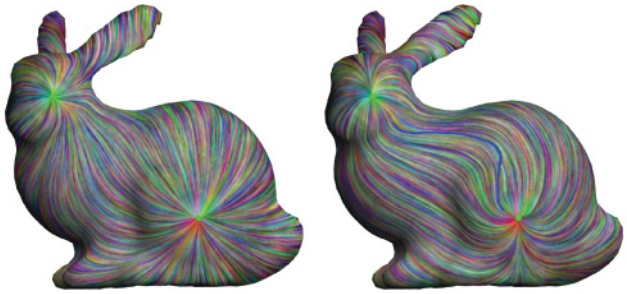

(a) Original vector field (b) With a user-specified stroke

Fig. 8. **Design by stroke.** (a) From an n-vector or n-direction field with arbitrary singularities, (b) the user can draw a stroke (blue) in order to easily influence the direction of the field. The result is updated interactively by solving the linear system resulting from the variational approach of Section 7.1.

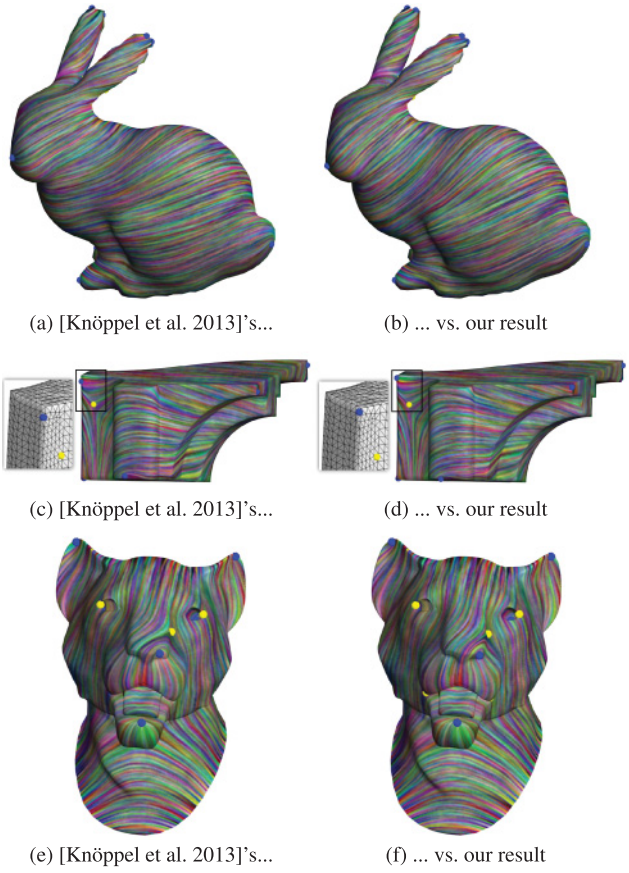

(a) [Knöppel et al. 2013]'s... (b) ... vs. our result

(c) [Knöppel et al. 2013]'s... (d) ... vs. our result

(e) [Knöppel et al. 2013]'s... (f) ... vs. our result

Fig. 9. **Comparisons.** While the method of Knöppel et al. [2013] finds similar singularities, our approach leads to "straighter" vector fields (see neck of bunny, (a) and (b); nose of lion, (e) and (f)), and the positions of our singularities are found closer to corners (see insets of fandisk, (c) and (d)). Yellow and blue markers indicate the presence of singularities in the vector fields.

7.2 Eigen Design

While our variational approach to editing is fast and simple, it suffers from two shortcomings: first, one needs to start from an existing vector field to begin the editing process; second, spurious singularities can appear as more constraints are input by the user. Both these issues can be addressed using a different approach to vector field editing, where a vector field is provided such that it is the "smoothest" field satisfying the constraints prescribed by the user. Indeed, Knöppel et al. [2013] noticed that the vector field with the lowest Dirichlet energy for a fixed L_2 norm can be found through a generalized eigenvalue problem (i.e., a Helmholtz equation) $\mathbf{Au} = \lambda\mathbf{Bu}$, which makes use of both the connection Laplacian matrix $\mathbf{A}$ (computing the Dirichlet energy E_D) and the mass matrix $\mathbf{B}$ (computing the L_2 norm, see Section 6.2). We can adopt this idea, but now using our discrete optimized connection—resulting in improved eigen vector fields with singularities appearing at more salient locations (see Figure 9).

However, our discrete operators for first-order derivatives offer a much more general extension of this design approach. Indeed, we can now modify the connection Laplacian matrix to add a quadratic penalty on the vector field components *along* user-specified strokes directly in the eigenvalue problem. This approach can be vastly preferable to the alignment constraint of Fisher et al. [2007], especially near singularities where forcing the magnitude of vectors may lead to artifacts. We propose to alter the generalized eigenvalue problem by changing $\mathbf{A}$ to represent the quadratic form for

$$\int_M |\nabla \mathbf{u}|^2 dA + w \int_c |\nabla_{\dot{c}}(\mathbf{u} - (\mathbf{u}\cdot\dot{c})\dot{c})|^2 ds,$$

where $c(.)$ is the user stroke with arclength parameterization s, and changing $\mathbf{B}$ to represent

$$\int_M |\mathbf{u}|^2 dA + w \int_c |\mathbf{u}\cdot\dot{c}|^2 ds.$$

With these modified matrices, we force the alignment to the stroke without restricting the magnitude (through the additional second term in A) and avoid the magnitude of the vectors along the stroke to be penalized (through the additional term in B)—see Figure 10. The user can then adjust the weight w to choose how closely the resulting vector field should follow the stroke.

Similarly, the mass matrix can be modified to control both singularity placement and orientation using the terms we presented in Section 7.1. Solving the resulting generalized eigenvalue problem provides the "smoothest" vector field that satisfies user constraints, where smoothest is defined with respect to the notion of connection used to derive the covariant derivative. If the user also changes the discrete connection to be trivial with prescribed singularities as described in Section 5.3, the vector field will be smoothest for this connection as demonstrated in Figure 11. From this eigen design, variational editing (Section 7.1) can be performed if the user wishes to further edit the vector field. The added flexibility that the assignment of strokes and singularities offers significantly increases the applicability of this eigen approach to the design of direction fields.

8. RESULTS

We present numerical tests of the accuracy of our operators derived from our discrete connection as well as a few vector field design results using our two approaches.

8.1 Accuracy of Discrete Operators

We evaluate the accuracy of the discrete approximations of div, curl, and $\bar{\partial}$ per triangle. To allow for proper error evaluation, we use a set of triangle meshes interpolating a sphere at various levels of discretization and use a smooth vector field (namely, a low-order vector spherical harmonic) with a known expression so that we

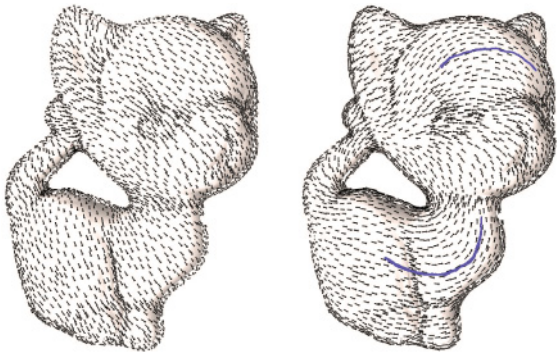

(a) Smoothest vector field for the Levi-Civita connection, no constraints added.

(b) Smoothest vector field for the Levi-Civita connection that matches a user-specified stroke.

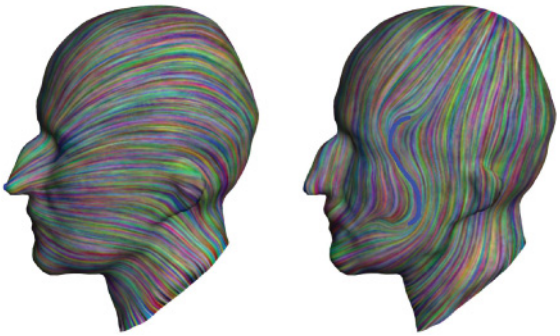

(c) Smoothest vector field for the Levi-Civita connection, no constraints added.

(d) Smoothest vector field for the Levi-Civita connection that matches a user-specified stroke.

Fig. 10. **Eigen design.** While an unconstrained generalized eigenvalue problem ((a) and (c)) will result in the smoothest vector field (i.e., with the lowest Dirichlet energy for a fixed L_2 norm) for the as-Levi-Civita-as-possible connection, we can also find the smoothest vector field that matches user-specified strokes ((b) and (d)), offering a very intuitive design tool.

(a) Smoothest vector field for the Levi-Civita connection, with no constraints added

(b) Smoothest vector field (for the Levi-Civita connection) that matches a user-specified stroke

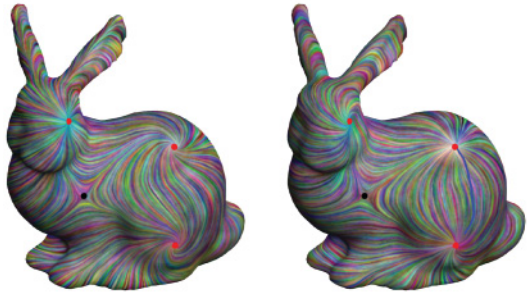

(c) Smoothest vector field for a trivial connection (with prescribed singularities) with no added constraints

(d) Smoothest vector field (for the same trivial connection of (c)) that matches a user-specified stroke

Fig. 11. **Eigen design with trivial connections.** While unconstrained generalized eigenvalue problems can be used to find the smoothest vector fields for the as-Levi-Civita-as-possible connection with or without stroke constraints ((a) and (b)), the user can also prescribe a trivial connection (c) with given singularities (both positive and negative, placed on the singularities of (a) here); stroke constraints can also be added (d).

can evaluate its exact divergence and curl everywhere. We then compute the L_2 and L_∞ errors between our discrete divergence (curl, respectively) evaluation and the real integral value per triangle. The results shown in Table I demonstrate that our optimization of the connection impacts the accuracy of first-order operators quite significantly compared to a geodesic polar-map-based connection. The area-based versus edge-based evaluations of the local first-order derivatives presented in Section 6.3 are, however, minimally different. We found that the Stokes approach (based on ω_e) often leads to a better accuracy especially on fine meshes; yet, the area-based operators are slightly more robust to noise as they rely on area versus edge integrals. We used the same setup to evaluate the accuracy of our vector field energies based on our triangle-based first-order derivatives, and once again the optimized connection shows superior numerical accuracy—except on very coarse meshes.

Our Dirichlet energy results are also systematically better than the L_2 evaluation provided by Knöppel et al. [2013], even when our optimal vertex-to-vertex connection angles ρ_{ij} are used to improve their results. The difference of the antiholomorphic and holomorphic energies for direction fields is also a good measure of accuracy, as we know that it should evaluate to the Euler characteristic of the mesh times 2π, and the edge-based evaluations using our optimized connections exhibit, once again, significantly improved accuracy as shown in Table II. Our operators are thus well suited to vector field analysis on manifold simplicial complexes.

8.2 Vector and n-Direction Field on Meshes

We experimented with our variational-based editing approach based on the quadratic energy P. As expected, this simple numerical method (requiring only a linear solve for each new constraint added by the user) offers control not only over positive singularities but also over saddle points in the vector field and their principal axes. For instance, a saddle point happening on the side of a mesh (see Figure 6) can be rotated by any angle without changing its position. The same control applies to n-direction fields without any code modification (see Figure 5).

Finally, we tried our eigen approach to vector field design. First, we found that our notion of smoothest vector field for the Levi-Civita connection is quite close to the results of Knöppel et al. [2013], although visual comparisons show from marginal to moderate improvements depending on the complexity of the model (see Figure 9). Where our method *really* differs is in our ability to handle user constraints in the exact same framework as demonstrated in Figure 10, as well as arbitrary connections as shown in Figure 11.

Table I. **Approximation Errors**

Using meshes of increasing resolutions that all interpolate a sphere, we evaluate the L_2 and L_∞ errors for the divergence (top and middle left) and curl (top and middle right), and dirichlet energy operators (bottom) evaluated per triangle using our edge-based approach (via stokes). The sphere mesh has only 162 vertices, and we refine ts connectivity via loop subdivisions, leading to meshes of 642, 2,562, and 10,242 vertices. We averaged the errors incurred for 100 random vector fields that are linear combinations of the first 40 vector spherical harmonics, normalized to ave Unit L_2 norm. The optimal (as-Levi-Civita-as-possible) connection systematically produces the smallest error except for extremely coarse resolutions. We also improve on the L_2 norm produced by Knöppel et al. [2013], even when our (locally optimal) vertex-to-vertex angles ρ_{ij} are used in their formulae.

L_2 Error for Div	Polar Map	Local Optimal	Global Optimal
sphere	0.2447	0.2239	**0.1809**
sphere Loop 1	0.1586	0.1054	**0.0361**
sphere Loop 2	0.2742	0.1297	**0.0084**
sphere Loop 3	0.7746	0.2749	**0.0020**

L_2 Error for Curl	Polar Map	Local Optimal	Global Optimal
sphere	0.2453	0.2251	**0.1823**
sphere Loop 1	0.1563	0.1039	**0.0361**
sphere Loop 2	0.2760	0.1300	**0.0083**
sphere Loop 3	0.7765	0.2752	**0.0020**

L_∞ Error for Div	Polar Map	Local Optimal	Global Optimal
sphere	0.5752	0.3690	**0.2978**
sphere Loop 1	1.0984	0.5613	**0.1280**
sphere Loop 2	1.6928	0.9602	**0.0602**
sphere Loop 3	3.6589	3.2195	**0.0240**

L_∞ Error for Curl	Polar Map	Local Optimal	Global Optimal
sphere	0.4898	0.5130	**0.3294**
sphere Loop 1	0.8183	0.5225	**0.1321**
sphere Loop 2	2.0324	1.0027	**0.0604**
sphere Loop 3	3.9119	2.0779	**0.0240**

L_2 Error for E_D	Polar Map	Local Optimal	Global Optimal
sphere	**2.1906**	2.2470	2.4016
sphere Loop 1	**0.2306**	0.3613	0.6258
sphere Loop 2	0.8679	0.3259	**0.1581**
sphere Loop 3	3.0080	1.0464	**0.0396**

Knöppel et al. [2013]	Knöppel et al. [2013] w/ Optimal ρ_{ij}
2.4161	2.4153
0.6300	0.6298
0.1592	0.1591
0.0399	0.0398

Table II. **Approximations of Euler Characteristic**

For a pointwise unit vector field $\mathbf{u}$, the difference of antiholomorphic and holomorphic energies is $E_{\mathrm{A}}(\mathbf{u}) - E_{\mathrm{H}}(\mathbf{u}) = \int_{\mathcal{T}} K$ (Equation (5)). Using random linear combinations of the 30 lowest vector spherical harmonics, we evaluate the difference of our discrete energies E_A and E_H for 100 vector fields (with unit norm at each vertex), divided by π; we indicate both the mean and the standard deviation of these 100 integrations. On various meshes (of genus 0 and 2), our edge-based evaluations exhibit significantly lower errors than all other area-based estimations, including results from Knöppel et al. [2013].

$\int_{\mathcal{T}} K$ (mean/std)	Polar Map	Local Optimal	Global Optimal	Knöppel et al. [2013]	Global Optimal w/ Stokes
sphere	$3.9730/0.923e^{-3}$	$3.9756/0.623e^{-3}$	$3.9756/0.619e^{-3}$	$3.9756/0.620e^{-3}$	**4.0000**$/0.000e^{-3}$
sphere Loop 1	$3.9878/0.341e^{-3}$	$3.9897/0.102e^{-3}$	$3.9898/0.103e^{-3}$	$3.9898/0.103e^{-3}$	**4.0000**$/0.000e^{-3}$
sphere Loop 2	$3.9948/0.455e^{-3}$	$3.9970/0.057e^{-3}$	$3.9970/0.057e^{-3}$	$3.9970/0.057e^{-3}$	**4.0000**$/0.000e^{-3}$
bunny	$3.8857/0.850e^{-2}$	$3.9082/0.706e^{-2}$	$3.9192/0.741e^{-2}$	$3.9193/0.742e^{-2}$	**3.9995**$/0.000e^{-3}$
bunny Loop	$3.9610/1.199e^{-2}$	$3.9860/0.696e^{-2}$	$3.9880/0.725e^{-2}$	$3.9875/0.725e^{-2}$	**4.0003**$/0.000e^{-3}$
torus	$0.0234/0.913e^{-2}$	$0.0216/0.371e^{-2}$	$0.0207/0.381e^{-2}$	$0.0207/0.381e^{-2}$	**-0.0003**$/0.000e^{-3}$
torus Loop	$-0.0025/0.328e^{-2}$	$-0.0022/0.059e^{-2}$	$-0.0013/0.065e^{-2}$	$-0.0016/0.065e^{-2}$	**0.0000**$/0.000e^{-3}$

8.3 Timings

Our vector field design shares the exact same timings as the works it extends [Fisher et al. 2007; Knöppel et al. 2013]. For instance, a typical mesh of $50K$ triangles requires around $5s$ for matrix factorization, around $0.5s$ when the variational approach of Section 7.1 is used (incremental updates of the design take considerably less), and around $1s$ when the eigen design of Section 7.2 is used instead. However, our approach requires the computation of the as-Levi-Civita-as-possible connection as a processing step, adding $1.5s$ to solve the linear system described in Section 5.3.

9. CONCLUSION

We have proposed the construction of a discrete notion of connection and its covariant derivative by exploiting the simplicial nature of triangulated 2-manifolds and picking the lowest-order finite element basis functions we could (to simplify the resulting expressions and make vector field design as efficient as possible) such that derivatives and their L_2 norms are well defined and finite. The resulting discrete covariant derivative is linear and metric preserving by definition, although it fails to exactly satisfy Leibniz's rule as most Whitney-based discrete operators. Our notion of discrete connection was shown to be numerically superior to previous approaches, and applications to vector and direction field design were demonstrated.

In the future, we believe that various applications in geometry processing (such as integral lines) and even simulation would benefit from a smoother approximation. Higher-order connections that still fit our framework could be derived from subdivision-based Whitney forms defined in Wang et al. [2006] or from other higher-order

Whitney forms—as long as their integrals can be either evaluated in closed form or through quadrature.

APPENDIX

A. EXPLICIT EVALUATION OF OPERATORS

In this appendix, we describe how one encodes our discrete operators for a vector field $\mathbf{u}$ as matrices acting on the vector components (u_i^1, u_i^2) at each vertex v_i. We adopt the following shorthand notation for clarity: $\rho \equiv \rho_{v_i \to e_{ij}}$, $\epsilon \equiv \epsilon_{ij}$, and $\theta \equiv \angle(\mathbf{e}_{e_{ij}}, \mathbf{e}_{t_{ijk}})$.

A.1 Divergence/Curl for n-Vector Fields

When all the local frames in the neighborhood rotate by $-\alpha$, the representative vector field $\mathbf{v}$ of an n-vector field can be expressed in the new frame as $\mathbf{v}' = \exp(Jn\alpha)\mathbf{v}$. The covariant derivative with respect to an arbitrary vector field $\mathbf{w}$ $\nabla_{\mathbf{w}}\mathbf{v} = (\nabla\mathbf{v})\mathbf{w}$ also changes expression as an n-vector field, yielding

$$\exp(Jn\alpha)(\nabla\mathbf{v})\mathbf{w} = (\nabla\mathbf{v}')\mathbf{w}' = (\nabla\mathbf{v}')\exp(J\alpha)\mathbf{w}.$$

Applying Equation (4) and noting that $F\exp(J\alpha) = \exp(-J\alpha)F$,

$$\begin{aligned}\nabla\mathbf{v}' &= \exp(Jn\alpha)(\nabla\mathbf{v})\exp(-J\alpha)\\ &= \frac{1}{2}\exp(Jn\alpha)(\partial\mathbf{v} + F\bar{\partial}\mathbf{v})\exp(-J\alpha)\\ &= \frac{1}{2}\exp(J(n-1)\alpha)\partial\mathbf{v} + \frac{1}{2}\exp(J(n+1)\alpha)F\bar{\partial}\mathbf{v}.\end{aligned}$$

Thus, $\partial\mathbf{v}$ transforms as an $(n-1)$-vector field, while $\bar{\partial}\mathbf{v}$ transforms as an $(n+1)$-vector field.

A.2 Edge-Based Operators

Our discrete operators are each represented as a $|F| \times 2|V|$ matrix, assembled based on the contribution of the vector components at each vertex v_i to the integral value of the operator on each adjacent triangle t_{ijk}. Through integration by parts, we find

$$\begin{aligned}\int_{e_{ij}} \Psi_i dl &= |e_{ij}| \int_0^1 (1-x)\exp(-J(\epsilon x + \rho))dx\\ &= \frac{|e_{ij}|}{\epsilon^2}\exp(-J\rho)[I - J\epsilon - \exp(-J\epsilon)].\end{aligned}$$

We can now evaluate the four discrete operators through the following function:

$$I(\rho, \epsilon) = \frac{|e_{ij}|}{\epsilon^2 |t_{ijk}|}[\cos(\rho) - \cos(\rho+\epsilon) - \sin(\rho)\epsilon].$$

If we denote by $\mathrm{op}_{t_{ijk}}^{u_i^m}$ the contribution of the mth component of $\mathbf{u}_i$ to the integral of operator op in t_{ijk}, we have (recall that for an n-vector field, divergence and curl operators produce an $(n-1)$-vector field, while the reflected ones produce an $(n+1)$-vector field, see Appendix A):

$$\begin{aligned}\mathrm{curl}\ {}^{u_i^1}_{t_{ijk}} &= I(n\rho + (n-1)\theta, n\epsilon),\\ \mathrm{curl}\ {}^{u_i^2}_{t_{ijk}} &= I(n\rho + (n-1)\theta| + \pi/2, n\epsilon),\\ \mathrm{div}\ {}^{u_i^1}_{t_{ijk}} &= I(n\rho + \pi/2 + (n-1)\theta, n\epsilon),\\ \mathrm{div}\ {}^{u_i^2}_{t_{ijk}} &= I(n\rho + \pi/2 + (n-1)\theta, n\epsilon),\\ \overline{\mathrm{curl}}\ {}^{u_i^1}_{t_{ijk}} &= I(n\rho + (n+1)\theta, n\epsilon),\\ \overline{\mathrm{curl}}\ {}^{u_i^2}_{t_{ijk}} &= I(n\rho + (n+1)\theta + \pi/2, n\epsilon),\\ \overline{\mathrm{div}}\ {}^{u_i^1}_{t_{ijk}} &= I(n\rho + (n+1)\theta + \pi/2, n\epsilon),\\ \overline{\mathrm{div}}\ {}^{u_i^2}_{t_{ijk}} &= I(n\rho + (n+1)\theta + \pi, n\epsilon).\end{aligned}$$

A.3 Triangle-Based Operators

We evaluated the per-triangle integral expressions of our operators through symbolic integration. Note that it leads to expressions with $\tau_{ij,k}$, $\tau_{jk,i}$, and $\tau_{ki,j}$ appearing in the denominator. As these values can be close to zero, Chebyshev [Knöppel et al. 2013] or Taylor expansion is typically necessary to provide robustness in evaluation.

ACKNOWLEDGMENTS

This work was completed in January 2014, and we are grateful to Patrick Mullen for proofreading the first version of this article, Max Budninskiy for comments, and Santiago Lombeyda for his timely help with figures. Visualization of vector fields was done using the code from Palacios and Zhang [2007]. The authors also acknowledge funding from NSF grants CCF-1011944, IIS-0953096, CMMI-1250261, and III-1302285, and the support of Pixar Animations Studios, Disney Animation Studios, and Google. MD gratefully thanks the Inria International Chair program and all the members of the TITANE team for support. YT thanks the CAD/CG State Key Lab at Zhejiang University for support.

REFERENCES

R. Abraham, J. E. Marsden, and R. Ratiu. 1988. *Manifolds, Tensor Analysis, and Applications,* 2nd ed. Springer-Verlag.

David Bommes, Henrik Zimmer, and Leif Kobbelt. 2009. Mixed-integer quadrangulation. *ACM Trans. Graph.* 28, 3 (2009), 77:1–77:10.

Keenan Crane, Mathieu Desbrun, and Peter Schröder. 2010. Trivial connections on discrete surfaces. *Comp. Graph. Forum* 29, 5 (2010), 1525–1533.

Fernando de Goes, Beibei Liu, Max Budninskiy, Yiying Tong, and Mathieu Desbrun. 2014. Discrete 2-tensor fields on triangulations. *Comp. Graph. Forum* 33, 5 (2014), 13–24.

Mathieu Desbrun, Eva Kanso, and Yiying Tong. 2008. Discrete differential forms for computational modeling. In *Discrete Differential Geometry*, A. I. Bobenko, P. Schröder, J. M. Sullivan, and G. M. Ziegler (Eds.). Oberwolfach Seminars, Vol. 38. Birkhäuser Basel, 287–324.

Matthew Fisher, Peter Schröder, Mathieu Desbrun, and Hugues Hoppe. 2007. Design of tangent vector fields. *ACM Trans. Graph.* 26, 3 (2007), 56:1–56:9.

Cindy M. Grimm and John F. Hughes. 1995. Modeling surfaces of arbitrary topology using manifolds. In *Proc. ACM SIGGRAPH Conf.* 359–368.

Aaron Hertzmann and Denis Zorin. 2000. Illustrating smooth surfaces. In *Proc. ACM SIGGRAPH Conf.* 517–526.

Scott Kircher and Michael Garland. 2008. Free-form motion processing. *ACM Trans. Graph.* 27, 2 (2008), 12:1–12:13.

M. S. Knebelman. 1951. Spaces of relative parallelism. *Annals of Mathematics* (1951), 387–399.

Felix Knöppel, Keenan Crane, Ulrich Pinkall, and Peter Schröder. 2013. Globally optimal direction fields. *ACM Trans. Graph.* 32, 4 (2013), 59:1–59:10.

Yaron Lipman, Olga Sorkine, David Levin, and Daniel Cohen-Or. 2005. Linear rotation-invariant coordinates for meshes. *ACM Trans. Graph.* 24, 3 (2005), 479–487.

Beibei Liu, Yanlin Weng, Jiannan Wang, and Yiying Tong. 2013. Orientation field guided texture synthesis. *J. Comp. Sci. Tech.* 28, 5 (2013), 827–835.

Kishore Marathe. 2010. *Topics in Physical Mathematics*. Springer Science.

Ashish Myles, Nico Pietroni, and Denis Zorin. 2014. Robust field-aligned global parametrization. *ACM Trans. Graph.* 33, 4 (2014), 135:1–135:8.

Ashish Myles and Denis Zorin. 2013. Controlled-distortion constrained global parametrization. *ACM Trans. Graph.* 32, 4 (2013), 105:1–105:14.

Jonathan Palacios and Eugene Zhang. 2007. Rotational symmetry field design on surfaces. *ACM Trans. Graph.* 26, 3 (2007), 55:1–55:10.

Daniele Panozzo, Yaron Lipman, Enrico Puppo, and Denis Zorin. 2012. Fields on symmetric surfaces. *ACM Trans. Graph.* 31, 4 (2012), 111:1–111:12.

Konrad Polthier and Eike Preuß. 2000. Variational approach to vector field decomposition. In *Data Visualization*. 147–155.

Konrad Polthier and Eike Preuß. 2003. Identifying vector field singularities using a discrete Hodge decomposition. In *Vis. and Math. III*, Hans-Christian Hege and Konrad Polthier (Eds.). Springer Verlag, 113–134.

Nicolas Ray and Dmitry Sokolov. 2014. Robust polylines tracing for n-symmetry direction field on triangle surfaces. *ACM Trans. Graph.* 33, 3 (2014), 30:1–30:8.

Nicolas Ray, Bruno Vallet, Laurent Alonso, and Bruno Levy. 2009. Geometry-aware direction field processing. *ACM Trans. Graph.* 29, 1 (2009), 1:1–1:11.

Nicolas Ray, Bruno Vallet, Wan Chiu Li, and Bruno Lévy. 2008. N-symmetry direction field design. *ACM Trans. Graph.* 27, 2 (2008), 10:1–10:13.

Michael Spivak. 1979. *A Comprehensive Introduction to Differential Geometry. Vol. II*, 2nd ed. Publish or Perish.

Holger Theisel. 2002. Designing 2d vector fields of arbitrary topology. *Comp. Graph. Forum* 21, 3 (2002), 595–604.

Yiying Tong, Santiago Lombeyda, Anil N. Hirani, and Mathieu Desbrun. 2003. Discrete multiscale vector field decomposition. *ACM Trans. Graph.* 22, 3 (2003), 445–452.

Ke Wang, Weiwei, Yiying Tong, Mathieu Desbrun, and Peter Schröder. 2006. Edge subdivision schemes and the construction of smooth vector fields. *ACM Trans. Graph.* 25, 3 (2006), 1041–1048.

Y. Wang, B. Liu, and Y. Tong. 2012. Linear surface reconstruction from discrete fundamental forms on triangle meshes. *Comp. Graph. Forum* 31, 8 (2012), 2277–2287.

H. Whitney. 1957. *Geometric Integration Theory*. Princeton University Press.

Eugene Zhang, Konstantin Mischaikow, and Greg Turk. 2006. Vector field design on surfaces. *ACM Trans. Graph.* 25, 4 (2006), 1294–1326.

Received August 2014; revised November 2015; accepted December 2015